AIAA JOURNAL
Vol. 47, No. 1, January 2009

Dynamic Aeroelasticity of Structurally Nonlinear Configurations Using Linear Modally Reduced Aerodynamic Generalized Forces

Luciano Demasi*
San Diego State University, San Diego, California 92182-1308
and
Eli Livne†
University of Washington, Seattle, Washington, 98195-2400

DOI: 10.2514/1.34797

Steady-state and time-domain methods are introduced for integrating commonly used frequency-domain unsteady aerodynamic modeling based on a modal approach with full-order finite element models for structures with geometric nonlinearities. The methods are aimed at airplane configurations in which geometric-stiffness effects are important but deformations are moderate, flow is attached, and linear unsteady aerodynamic modeling is adequate, such as joined-wing and strut-braced wings at small-to-moderate angles of attack or a low-aspect-ratio wing. The approach proposed in this paper is to use the full-order structural matrices to capture the nonlinear structural behavior and modally reduced aerodynamic matrices calculated by adopting a frequency-domain-based commercial code such as ZAERO or a doublet-lattice method or linearized modal-based generalized aerodynamic matrices generated by computational fluid dynamics codes.

I. Introduction

ALTHOUGH addressed rigorously for years in helicopter rotor aeroelasticity, structural nonlinearity due to large deformation and geometric-stiffness effects was not considered to be a major factor in the aeroelasticity of conventional fixed-wing configurations. Using nonlinear-beam models, the aeroelasticity of geometrically nonlinear high-aspect-ratio configurations was studied in the 1970s and 1980s, focusing on gliders and human-powered vehicles [1–3].

With the subsequent appearance of high-altitude long-endurance unmanned aerial vehicles, renewed interest in the nonlinear aeroelastic effects of large deformation led to additional research based on the coupling of nonlinear-beam models with essentially 2-D unsteady aerodynamics, suitable for the modeling of configurations of very high aspect ratios [4–10].

Other configurations affected structurally by geometric nonlinear behavior also emerged: more recently, the strut-braced wing [11–13] and, earlier, the joined-wing configuration [14–20].

Interest in aeroelastic limit cycle oscillation (LCO) behavior, with an initial focus on the contribution of control-surface free play and the behavior of thin fighter wings carrying external stores, led to a search for other possible structural nonlinearities that may cause LCO, such as the stiffening of plate structures subject to large deformation. Theoretical and experimental studies of platelike and beamlike wings with geometric structural nonlinearity [21–24] have indeed confirmed the importance of understanding when structural geometric nonlinear effects become aeroelastically important and accounting for them.

Most of the nonlinear aeroelastic modeling work done to date in the structural area was based on nonlinear-beam or Ritz-plate models to account for large deformations. These models are very useful for modeling simple wind-tunnel models or very-high-aspect-ratio wings, but they cannot be used to model general configurations, and their major limitation is their inability to capture local effects. Such local effects include the behavior at and around joints and the calculation of reliable stress information, especially in areas of high stress concentration. Nonlinear finite elements can allow capturing such local effects and modeling of general configurations at complexity levels that can represent real airplanes. But in the very few cases in which nonlinear finite elements were used to model a geometrically nonlinear structure, they were coupled with computational fluid dynamics (CFD) models for the flow. This was done for static aeroelastic modeling using sequential application of nonlinear structural and CFD models. Capabilities that couple nonlinear finite elements in an integrated manner with steady and unsteady CFD aerodynamics already exist [25,26], but they require a lengthy model setup and meshing process as well as considerable computational resources.

Because time-domain modeling is required for capturing both stability and dynamic response behavior (especially gust response) of nonlinear aeroelastic systems, appropriate unsteady aerodynamic modeling also becomes a challenge. In the case of high-aspect-ratio configurations and structural geometric nonlinearity, as stated before, 2-D linear potential unsteady aerodynamic models in the time domain are used with considerable success to capture aeroelastic behavior in subsonic flow [27]. Such models can be used to also model dynamic-stall effects [28]. For low-aspect-ratio wings, for which deformation is small enough that the unsteady aerodynamic loads are linear but large enough to cause structural geometric nonlinearity, dedicated time-marching vortex-lattice models proved to be adequate [22–24]. These dedicated time-marching vortex-lattice models are limited to planar configurations of simple planforms and to incompressible flow.

Linear compressible unsteady aerodynamic theory, the foundation of aeroelastic analysis and clearance of all flight vehicles flying today, has not been used so far for the aeroelastic modeling of structurally nonlinear airplanes. Computer capabilities such as the doublet-lattice-method (DLM) codes [29–38], PANAIR [39],

Presented as Paper 2105 at the 48th AIAA/ASME/ASCE/AHS/ASC Structures, Structural Dynamics, and Materials Conference, Honolulu, HI, 23–26 April 2007; received 25 September 2007; revision received 10 February 2008; accepted for publication 17 February 2008.

*Assistant Professor, Department of Aerospace Engineering and Engineering Mechanics; ldemasi@mail.sdsu.edu. Member AIAA.

†Professor, Department of Aeronautics and Astronautics, Box 352400; eli@aa.washington.edu. Associate Fellow AIAA.

ZAERO [40–42], and other linear potential aerodynamic codes are used and are still being used successfully in aeroelastic analyses of flight vehicles over a wide range of flight conditions. These codes can be used to model general three-dimensional configurations made of lifting surfaces, control surfaces, fuselages, nacelles, external stores, etc. One problem is that they are based on a frequency-domain formulation, in which unsteady aerodynamic-force terms are calculated for simple harmonic motion at given reduced frequencies. These need to be transformed to the time domain for integration with time-domain nonlinear structural models. But the main problem with the use of linear unsteady aerodynamic codes for the aeroelastic modeling of structures with geometric nonlinearities is that they are tailored for a modal approach. That is, these codes produce generalized unsteady aerodynamic-force terms for a set of mode shapes of motion given as input.

In a modern modal approach, the detailed finite element model of a structural dynamics system is reduced in order by describing the motion using a superposition of mode-shape vectors. The problem with this approach in the case of geometrically nonlinear structures, or any structural system for that matter, is that when local effects become important and unpredictably spread, the modal approach usually fails. Successful modal-order reduction of structural models in the linear case can be achieved in the case of strong local effects when the location of these effects is known a priori; the structural nonlinear case, however, is different. Because of the dependence of geometric-stiffness matrices on stress distributions and because of the large changes such stress distributions can portray as loading increases and the structure approaches instability, modal-order reduction tends to fail when used to reduce the order of general structures undergoing large deformation. The case of the joined-wing configuration is even more severe. Concentrated loads transferred through the joint connecting the main wing and the rear wing attached to it affect stress distributions around the joint area. The structural dynamics of the configuration are extremely sensitive to the location and details of the joint design. Studies of the nonlinear structural dynamics of this configuration using a number of modal-order-reduction approaches showed failure of all those approaches to yield accurate reduced-order structural dynamics models capable of capturing both displacement and stress behavior [43].

Both joined-wing and strut-braced wing configurations display strong geometrically nonlinear structural dynamics behavior, even without the large deformation typical in high-altitude long-endurance (HALE) vehicle wings. For attached-flow conditions that are typical of high-dynamic-pressure straight and level or maneuvering flight, the unsteady aerodynamics of such configurations are expected to be properly modeled by potential linear unsteady aerodynamic methods: the same methods used for the aeroelastic simulation of conventional configurations in compressible subsonic and supersonic flows. It is then important to develop the capability to simulate aeroelastic structurally nonlinear configurations of flight vehicles using an integration of nonlinear structural finite element models in full order (to avoid the difficulties with modal reduction in this case) with the standard linear modally based unsteady aerodynamic models, which can be used to model general configurations and for which significant experience exists.

The present paper will present such a modeling capability for investigating nonlinear aeroelastic problems of planar and nonplanar wing systems in general and of joined-wing configurations in particular. Integration of the nonlinear structural finite element (FE) capability with linear steady and linearized unsteady aerodynamic models will be discussed, as well as static and dynamic aeroelastic solution techniques. The conceptual description of the proposed procedure is shown in Fig. 1.

Studies in which coupling of full-order nonlinear finite element models with generalized aerodynamic-force models was compared with coupling of full-order nonlinear finite element models with full-order aerodynamic panel methods have been presented [44] before, with focus on the steady case; that formulation has now been revised and modified and it is extended here to the unsteady cases. In particular, generalized aerodynamic-force matrices produced by standard linear unsteady aerodynamic codes are transformed to the time domain and used with full-order structurally nonlinear finite element models to simulate time-dependent nonlinear aeroelastic behavior.

II. Terminology

The two quantities of displacement vector and cumulative-displacement vector will be used in both static and dynamic cases. They are introduced here for the steady case first, for the sake of simplicity. The displacement vector $\boldsymbol{u}^{\text{step}\lambda\text{iter}n}$ is referred to the configuration at the beginning of the current iteration n of load step λ in the Newton–Raphson procedure. The vector that contains the coordinates of all the structural nodes of the wing system will be $\boldsymbol{x}^{\text{step}\lambda\text{iter}n}$. The coordinates are relative to the configuration before the displacement vector is added. We will use an updated Lagrangian formulation [45–47], and so the coordinates of the nodes will be continuously updated during the iteration process.

The quantity $\boldsymbol{x}^{\alpha=0}$ represents the coordinate vector of all structural nodes at a reference aerodynamic configuration with no angle of

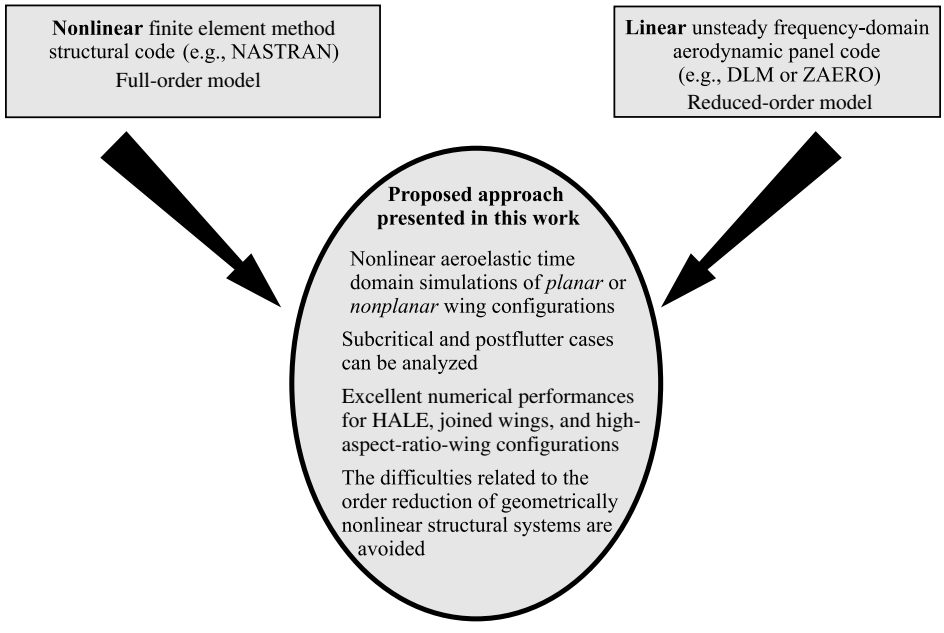

Fig. 1 Proposed approach for nonlinear aeroelastic time-domain simulations.

attack. Aerodynamic panels are defined based on the geometry of that reference configuration, and structural motion away from the reference configuration is small.

The concept of cumulative-displacement vector is also introduced. This quantity (indicated in the steady case with the symbol $\boldsymbol{U}^{\text{step}\lambda\text{iter}n}$) is defined as the summation of all the displacements that have occurred during the iteration process up to the current iteration. Basically, the coordinates at a particular load level are obtained by adding the vector of the coordinates in the undeformed configuration ($\boldsymbol{x}^{\alpha=0}$) to the translational part of all the displacements that the structure was subjected to during all of the previous load levels.

III. Present Doublet-Lattice Method

The doublet-lattice method is a very well-established procedure for the calculation of linear unsteady aerodynamic matrices in subsonic compressible flow [29–38]. In the present paper, a dedicated doublet-lattice code is developed. The approach is similar to that introduced by Sulaeman [13,37] to model the aerodynamic behavior at joined-wing joint areas. Basically, the unsteady aerodynamic kernel [48–50] is integrated using a Gaussian quadrature formula. To perform the calculation of the complicate kernels (expressed in Landhal's [49] form), Ueda's [51] formulas are adopted. A special procedure, similar to that introduced by Sulaeman [13] is used to isolate the singular part, and the integrals defined in the Hadamard finite-part sense [52,53] are analytically calculated. The use of the Gaussian quadrature formula allows the user to integrate the kernel with high accuracy. Therefore, the quality of the result is good, even for the steady case, and the use of a vortex-lattice approach (the typical approach used in the literature [32] when the steady case is studied with DLM) is not necessary. Validation of the present doublet-lattice code is done by comparing the results using different wing configurations reported in the literature [13,36,37,54,55]. In subsequent work, a standard [29] doublet-lattice approach was used.

It should be noted here that the proposed method will also work, after adaptation of proper aeromesh to structural mesh transformations, with linearized modal-based unsteady aerodynamic matrices created by CFD methods about reference configurations.

IV. Nonlinear Structural Model

The geometrically nonlinear structural model for thin-walled aerospace structures is created using flat triangular elements [45–47]. The tangent stiffness matrix is built adding the linear elastic stiffness matrix and the geometric-stiffness matrix. The geometric-stiffness matrix is derived by applying the load perturbation method: the gradient (with respect to the coordinates) of the nodal force vector (when the stresses are considered fixed) is calculated. The geometric-stiffness matrix is calculated adding 4 matrices [45–47]:

$$[\boldsymbol{K}_G^e]_{\text{total}}^{\text{shell}} = [\boldsymbol{K}_G^e]_{\text{IP}}^{\text{mem}} + [\boldsymbol{K}_G^e]_{\text{IP}}^{\text{plate}} + [\boldsymbol{K}_G^e]_{\text{out}}^{\text{mem}} + [\boldsymbol{K}_G^e]_{\text{out}}^{\text{plate}} \tag{1}$$

The matrix $[\boldsymbol{K}_G^e]_{\text{IP}}^{\text{mem}}$, representing the in-plane contribution of the plane-stress constant-strain triangular element, is obtained by taking the gradient of the nodal forces. The matrix $[\boldsymbol{K}_G^e]_{\text{IP}}^{\text{plate}}$, representing the in-plane contribution of the flat-triangular-plate bending element, is calculated using a similar approach applied to the triangular element based on the discrete Kirchoff theory. The matrix $[\boldsymbol{K}_G^e]_{\text{out}}^{\text{mem}}$, representing the out-of-plane contribution of the membrane, is calculated considering the change of a vector force that is subjected to a small rigid rotation vector $\boldsymbol{\omega}$. A similar approach is adopted to calculate the matrix $[\boldsymbol{K}_G^e]_{\text{out}}^{\text{plate}}$, which represents the out-of-plane contribution of the plate. A particular procedure [45] is then used to remove the rigid-body motion and calculate the unbalanced load as the analysis (Newton–Raphson) progresses.

V. Mesh-to-Mesh Transformations: Deformation Splining

A. Steady-Case Vortex-Lattice and Doublet-Lattice Methods

For linear potential steady and unsteady aerodynamics used in fixed-wing airplane aeroelasticity, only the component perpendicular to the surfaces is important. The aerodynamic modeling used here is based on aerodynamic reference surfaces with initial angles of attack that are zero, but with possibly nonzero dihedral angles. This is consistent with unsteady-aerodynamic-kernel function definitions used in lifting-surface theories.

The local x axis of an aerodynamic lifting surface is always the global x-axis direction of the flow. Each aerodynamic reference surface is divided into strips of panels. Low-order modeling is used, in which each panel has a load point and a control point. The DLM and vortex-lattice method (VLM) [56,57] use the same downwash and load points.

Let the 4 nodes that define a generic aerodynamic reference surface (denoted as a macropanel or wing segment) be denoted as 1^S, 2^S, 3^S, and 4^S (see Fig. 2). These points are chosen using the following rules:

$$x_1^S > x_2^S \qquad x_4^S > x_3^S \tag{2}$$

We start with the steady case, in which the load is increased gradually and a Newton–Raphson [58] procedure is used. A new incremental displacement vector $\boldsymbol{u}^{\text{step}\lambda\text{iter}n}$ is sought, which is referred to the deformed configuration $\boldsymbol{x}^{\text{step}\lambda\text{iter}n}$ reached in the previous iteration.

The wing system is divided into large trapezoidal aerodynamic reference surfaces. Each aerodynamic reference surface has to be associated with nodes on the structural mesh that affect its motion. That is done by referring both aerodynamic and structural nodes to the reference configuration and identifying the structural nodes associated with each wing segment.

$\boldsymbol{I}^S$ is the matrix that transforms the incremental displacements in global coordinates $\boldsymbol{u}^{\text{step}\lambda\text{iter}n}$ to the displacements of the only structural nodes on aerodynamic surface S. This matrix is not affected by the actual value of the displacements and depends on the identities of the nodes included in wing segment S; thus, this matrix is constant. The matrix $\boldsymbol{I}_d^S$ extracts the translational displacements on wing segment S; again, it is constant.

Using these two matrices, it is possible to express the translational displacement vector $\boldsymbol{u}_d^{S\text{step}\lambda\text{iter}n}$ (expressed in global coordinates) as follows:

$$\boldsymbol{u}_d^{S\text{step}\lambda\text{iter}n} = \boldsymbol{I}_d^S \cdot \boldsymbol{I}^S \cdot \boldsymbol{u}^{\text{step}\lambda\text{iter}n} \tag{3}$$

The vector $\boldsymbol{u}^{\text{step}\lambda\text{iter}n}$ contains all incremental displacements and node rotations of all nodes on the structures (i.e., all wing segments are included) referred to the deformation configuration $\boldsymbol{x}^{\text{step}\lambda\text{iter}n}$. The displacement vector $\boldsymbol{u}^{\text{step}\lambda\text{iter}n}$ has $6N_n$ components, where N_n is the number of all structural nodes in the model. The vector $\boldsymbol{u}_d^{S\text{step}\lambda\text{iter}n}$ has a dimension of $3N_n^S \times 1$, where N_n^S is the number of structural nodes on aerodynamic surface S that is being considered. The matrix $\boldsymbol{I}^S$ thus has the dimensions $6N_n^S \times 6N_n$, and the matrix $\boldsymbol{I}_d^S$ has the dimensions $3N_n^S \times 6N_n^S$.

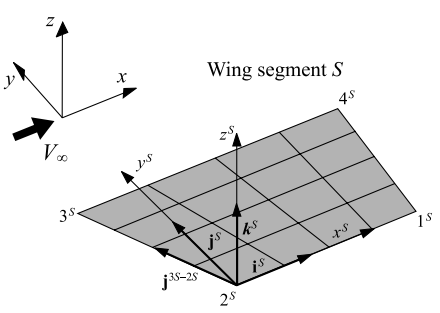

Fig. 2 Local coordinate system on an aerodynamic reference surface (which does not have an angle of attack).

At this point, we introduce the augmented-configuration nodal-coordinate vector $\bar{\boldsymbol{x}}^{\text{step}\lambda\text{iter}n}$, which is obtained by adding zero rows in places corresponding to rotational structural finite element degrees of freedom to the vector $\boldsymbol{x}^{\text{step}\lambda\text{iter}n}$, which contains the coordinates of the nodes of all wing systems. Thus, $\bar{\boldsymbol{x}}^{\text{step}\lambda\text{iter}n}$ can be formally treated as a finite element deformation vector, with 6 degrees of freedom associated with each node. The nodal-coordinate location vector of structural nodes included in wing surface S is then given by a relation that is identical to Eq. (3):

$$\boldsymbol{x}^{S\text{step}\lambda\text{iter}n} = \boldsymbol{I}_d^S \cdot \boldsymbol{I}^S \cdot \bar{\boldsymbol{x}}^{\text{step}\lambda\text{iter}n} \tag{4}$$

The matrices $\boldsymbol{I}_d^S$ and $\boldsymbol{I}^S$ are constant for the whole process.

The coordinates of the *final* location of structural nodes included in wing segment S are denoted as $\boldsymbol{X}^{S\text{step}\lambda\text{iter}n}$, and they are obtained by adding the coordinates of the nodes included in wing segment S with the translational displacements of the same nodes; these two quantities are calculated using Eqs. (3) and (4). The explicit form of the vector of nodal coordinates after the current iteration of a generic load step is completed is

$$\boldsymbol{X}^{S\text{step}\lambda\text{iter}n} = \boldsymbol{I}_d^S \cdot \boldsymbol{I}^S \cdot \bar{\boldsymbol{x}}^{\text{step}\lambda\text{iter}n} + \boldsymbol{I}_d^S \cdot \boldsymbol{I}^S \cdot \boldsymbol{u}^{\text{step}\lambda\text{iter}n} \tag{5}$$

To carry out splining transformation of motions from the structural to the aerodynamic mesh, structural and aerodynamic nodes are referred to the reference configuration, and it is necessary to define a coordinate system on the reference wing surface S (see Fig. 2). The vectors $\boldsymbol{i}^S$, $\boldsymbol{j}^S$, and $\boldsymbol{k}^S$ are expressed in the global coordinate system as

$$\begin{aligned} \boldsymbol{i}^S &= e_{11}^S \boldsymbol{i} + e_{12}^S \boldsymbol{j} + e_{13}^S \boldsymbol{k} \\ \boldsymbol{j}^S &= e_{21}^S \boldsymbol{i} + e_{22}^S \boldsymbol{j} + e_{23}^S \boldsymbol{k} \\ \boldsymbol{k}^S &= e_{31}^S \boldsymbol{i} + e_{32}^S \boldsymbol{j} + e_{33}^S \boldsymbol{k} \end{aligned} \tag{6}$$

Therefore, it is possible to define a 3×3 matrix $\boldsymbol{e}^S$ that is a coordinate transformation matrix from global to local coordinates. This matrix contains the direction cosines [see Eq. (6)].

The global coordinates of points 2^S on the reference surface S are denoted as x_{2^S}, y_{2^S}, and z_{2^S}. The coordinates of each of the points on the wing segment S expressed in the local coordinate system are determined by subtracting the global coordinates of the point 2^S and multiplying the result by the matrix $\boldsymbol{e}^S$. We introduce the vector $\boldsymbol{x}_{2^S}$ (which has the dimensions $3N_n^S \times 1$),

$$\boldsymbol{x}_{2^S} = \begin{bmatrix} x_{2^S} & y_{2^S} & z_{2^S} & \dots & x_{2^S} & y_{2^S} & z_{2^S} \end{bmatrix}^T \tag{7}$$

and the matrix $\boldsymbol{E}^S$, which is a block diagonal matrix, where the matrix $\boldsymbol{e}^S$ is repeated for all the structural nodes of each wing segment. The coordinates of the structural points on wing segment S can be expressed in the local coordinate system as (note that the dimension of $\boldsymbol{E}^S$ is $3N_n^S \times 3N_n^S$)

$$\begin{aligned} \boldsymbol{X}_{\text{loc}}^{S\text{step}\lambda\text{iter}n} &= \boldsymbol{E}^S \cdot [\boldsymbol{X}^{S\text{step}\lambda\text{iter}n} - \boldsymbol{x}_{2^S}] = \boldsymbol{E}^S \cdot [\boldsymbol{I}_d^S \cdot \boldsymbol{I}^S \cdot \bar{\boldsymbol{x}}^{\text{step}\lambda\text{iter}n} \\ &\quad + \boldsymbol{I}_d^S \cdot \boldsymbol{I}^S \cdot \boldsymbol{u}^{\text{step}\lambda\text{iter}n} - \boldsymbol{x}_{2^S}] \end{aligned} \tag{8}$$

At this point, the dihedral angle of the reference surface S is calculated. All panels of this surface will have the same dihedral angle. The dihedral is important because it is used in the expressions of the unsteady kernel in the doublet-lattice method [49].

We need to calculate the corresponding final coordinates of the load points to know the coordinates of points at which the aerodynamic forces are applied: perpendicular to the reference surface and so in the local z direction. Local coordinates and slopes of the aerodynamic control points are also needed. All of these interpolations are performed by using the infinite plate spline method [42,59]. To calculate the aerodynamic incidence in each panel of the wing surface S, it is necessary to calculate the derivative of the configuration and deformation shapes with respect to the local x axis x^S (see Fig. 2). To do that, the local coordinates $\boldsymbol{Z}_{\text{loc}}^{S\text{step}\lambda\text{iter}n}$ in the z^S direction are isolated. Calling $\boldsymbol{I}_z^S$ the constant matrix, which allows extraction of the z^S component (the dimension of that matrix is $N_n^S \times 3N_n^S$), it is possible to write [see Eq. (8)]

$$\begin{aligned} \boldsymbol{Z}_{\text{loc}}^{S\text{step}\lambda\text{iter}n} &= \boldsymbol{I}_z^S \cdot \boldsymbol{X}_{\text{loc}}^{S\text{step}\lambda\text{iter}n} = \boldsymbol{I}_z^S \cdot \boldsymbol{E}^S \cdot [\boldsymbol{I}_d^S \cdot \boldsymbol{I}^S \cdot \bar{\boldsymbol{x}}^{\text{step}\lambda\text{iter}n} \\ &\quad + \boldsymbol{I}_d^S \cdot \boldsymbol{I}^S \cdot \boldsymbol{u}^{\text{step}\lambda\text{iter}n} - \boldsymbol{x}_{2^S}] \end{aligned} \tag{9}$$

Using the fitted-surface spline shape, it is possible to calculate the derivatives of such shape and the associated local angle of attack. Suppose that the ith structural point on wing segment S is considered. The local z coordinate of the point i will be $Z_{i\text{loc}}^S$, where the superscript stepλiter$n$ is dropped for simplicity in the equations (it will be reinstated later):

$$Z_{i\text{loc}}^S = Z_{i\text{loc}}^S(x_{i\text{loc}}^S, y_{i\text{loc}}^S) \tag{10}$$

Again, it has to be clear that $x_{i\text{loc}}^S$ and $y_{i\text{loc}}^S$ are the local coordinates of the point i at which the local z coordinate $Z_{i\text{loc}}^S$ is considered. We make the assumption that the displacements are not very large, and so the aerodynamic linear theory holds. Also under this assumption, it is reasonable to consider the local in-plane coordinates of the nodes, the load points, and the control points of a generic wing segment as being constant. Only the out-of-plane local displacement will change during the iteration process. With this hypothesis, all the splining matrices are constant and they can be calculated once.

For each structural point i of wing segment S, the corresponding $Z_{i\text{loc}}^S(x_{i\text{loc}}^S, y_{i\text{loc}}^S)$ is written as

$$Z_{i\text{loc}}^S = a_0^S + a_1^S x_{i\text{loc}}^S + a_2^S y_{i\text{loc}}^S + \sum_{j=1}^{N_n^S} F_j^S (r_{ij\text{loc}}^S)^2 \, \ell_n (r_{ij\text{loc}}^S)^2 \tag{11}$$

where

$$(r_{ij\text{loc}}^S)^2 = (x_{i\text{loc}}^S - x_{j\text{loc}}^S)^2 + (y_{i\text{loc}}^S - y_{j\text{loc}}^S)^2 \tag{12}$$

Equation (11) can be rewritten introducing the matrix $\boldsymbol{K}^S$, which is defined as

$$K_{ij}^S = (r_{ij\text{loc}}^S)^2 \, \ell_n (r_{ij\text{loc}}^S)^2 \tag{13}$$

Thus,

$$Z_{i\text{loc}}^S(x_{i\text{loc}}^S, y_{i\text{loc}}^S) = a_0^S + a_1^S x_{i\text{loc}}^S + a_2^S y_{i\text{loc}}^S + \sum_{j=1}^{N_n^S} F_j^S K_{ij}^S \tag{14}$$

setting (note that $\boldsymbol{Z}_{\text{loc}}^{S\star}$ is coincident with $\boldsymbol{Z}_{\text{loc}}^S$ except for the fact that three rows of zeros are added)

$$\begin{aligned} \boldsymbol{Z}_{\text{loc}}^{S\star} &= \begin{bmatrix} 0 & 0 & 0 & Z_{1\text{loc}}^S & Z_{2\text{loc}}^S & Z_{3\text{loc}}^S & \cdots & Z_{N_n^S\text{loc}}^S \end{bmatrix}^T \\ \boldsymbol{F}^S &= \begin{bmatrix} a_0^S & a_1^S & a_2^S & F_1^S & F_2^S & F_3^S & \cdots & F_{N_n^S}^S \end{bmatrix}^T \end{aligned} \tag{15}$$

and defining

$$\boldsymbol{G}^S = \begin{bmatrix} \boldsymbol{0} & \boldsymbol{R}^S \\ [\boldsymbol{R}^S]^T & \boldsymbol{K}^S \end{bmatrix} \tag{16}$$

Based on the spline formulation (details are omitted here, but can be found in the literature [42,59]),

$$\boldsymbol{Z}_{\text{loc}}^{S\star} = \boldsymbol{G}^S \boldsymbol{F}^S \tag{17}$$

Note that $\boldsymbol{R}^S$ has the dimensions $3 \times N_n^S$, $\boldsymbol{K}^S$ has the dimensions $N_n^S \times N_n^S$, $\boldsymbol{F}^S$ has the dimensions $(3 + N_n^S) \times 1$, and $\boldsymbol{G}^S$ has the dimensions $(3 + N_n^S) \times (3 + N_n^S)$. Inverting the relation expressed by Eq. (17), it is possible to find the $N_n^S + 3$ unknowns represented by the components of the vector $\boldsymbol{F}^S$:

$$\boldsymbol{F}^S = [\boldsymbol{G}^S]^{-1} \boldsymbol{Z}_{m\text{loc}}^{S\star} \tag{18}$$

The coefficients that have to be used for the spline are now known.

The wall tangency condition (WTC) is enforced at the aerodynamic control points. Let the local coordinates (in the

reference plane) of the ith control point be indicated with $\mathcal{X}^S_{i\text{loc}}$ and $\mathcal{Y}^S_{i\text{loc}}$. The coordinate $\mathcal{Z}^S_{i\text{loc}}$ in the direction of z^S of the ith control point will be calculated using the equation of the spline:

$$\mathcal{Z}^S_{i\text{loc}}(\mathcal{X}^S_{i\text{loc}}, \mathcal{Y}^S_{i\text{loc}}) = a^S_0 + a^S_1 \mathcal{X}^S_{i\text{loc}} + a^S_2 \mathcal{Y}^S_{i\text{loc}} + \sum_{j=1}^{N^S_n} F^S_j \mathcal{K}^S_{ij} \quad (19)$$

where

$$\mathcal{K}^S_{ij} = (\mathcal{R}^S_{ij\text{loc}})^2 \ln(\mathcal{R}^S_{ij\text{loc}})^2 \quad (20)$$

and

$$(\mathcal{R}^S_{ij\text{loc}})^2 = (\mathcal{X}^S_{i\text{loc}} - x^S_{j\text{loc}})^2 + (\mathcal{Y}^S_{i\text{loc}} - y^S_{j\text{loc}})^2 \quad (21)$$

The number of control points is the same as the number of aerodynamic panels N^S. To impose the boundary conditions, the derivatives with respect to x^S are required. In reality, there is no difference between x and x^S, because the reference surfaces do not have angles of attack; however, we keep here the notation x^S to designate that the local coordinate system of wing segment S is considered (see Fig. 3). Therefore, it is necessary to differentiate the spline equation with respect to x^S and to calculate the result in the local coordinates of the control points. The vector $\mathrm{d}\boldsymbol{\mathcal{Z}}^S_{\text{loc}}/\mathrm{d}x^S$ contains the slopes of the control points. $\boldsymbol{\mathcal{D}}^S$ is a matrix that, when multiplied by the vector containing the coefficients of the spline, gives the vector $\mathrm{d}\boldsymbol{\mathcal{Z}}^S_{\text{loc}}/\mathrm{d}x^S$. The explicit form of this matrix is not listed here and is straightforward to obtain. Using these definitions, the slopes can be written as functions of the coefficients of the spline fit:

$$\frac{\mathrm{d}\boldsymbol{\mathcal{Z}}^S_{\text{loc}}}{\mathrm{d}x^S} = \boldsymbol{\mathcal{D}}^S \boldsymbol{F}^S \quad (22)$$

Note that $\mathrm{d}\boldsymbol{\mathcal{Z}}^S_{\text{loc}}/\mathrm{d}x^S$ has the dimensions $N^S \times 1$, and $\boldsymbol{\mathcal{D}}^S$ has the dimensions $N^S \times (N^S_n + 3)$. Using Eq. (18), Eq. (22) can be written as

$$\frac{\mathrm{d}\boldsymbol{\mathcal{Z}}^S_{\text{loc}}}{\mathrm{d}x^S} = \boldsymbol{\mathcal{D}}^S \boldsymbol{F}^S = \boldsymbol{\mathcal{D}}^S [\boldsymbol{G}^S]^{-1} \boldsymbol{Z}^{S\star}_{\text{loc}} \quad (23)$$

Observing that the first three rows of $\boldsymbol{Z}^{S\star}_{\text{loc}}$ are zeros, it is possible to eliminate the first three columns of the matrix $[\boldsymbol{G}^S]^{-1}$ without changing the result. Defining $\boldsymbol{S}^S$ (the matrix $[\boldsymbol{G}^S]^{-1}$ with the first three columns eliminated) and defining $\boldsymbol{Z}^S_{\text{loc}}$ (the vector $\boldsymbol{Z}^{S\star}_{\text{loc}}$ without the first three rows), Eq. (23) can be rewritten as

$$\frac{\mathrm{d}\boldsymbol{\mathcal{Z}}^S_{\text{loc}}}{\mathrm{d}x^S} = \boldsymbol{\mathcal{D}}^S \boldsymbol{S}^S \boldsymbol{Z}^S_{\text{loc}} \quad (24)$$

Note that $\boldsymbol{S}^S$ has the dimensions $(N^S_n + 3) \times N^S_n$, and $\boldsymbol{Z}^S_{\text{loc}}$ has the dimensions $N^S_n \times 1$. Using Eq. (9), Eq. (24) can be written as (at this point, we reinstate the superscript stepλiter$n$ dropped earlier)

$$\frac{\mathrm{d}\boldsymbol{\mathcal{Z}}^{S\text{step}\lambda\text{iter}n}_{\text{loc}}}{\mathrm{d}x^S} = \boldsymbol{\mathcal{D}}^S \boldsymbol{S}^S \boldsymbol{I}^S_z \boldsymbol{E}^S [\boldsymbol{I}^S_d \cdot \boldsymbol{I}^S \cdot \bar{\boldsymbol{x}}^{\text{step}\lambda\text{iter}n} + \boldsymbol{I}^S_d \cdot \boldsymbol{I}^S \cdot \boldsymbol{u}^{\text{step}\lambda\text{iter}n} - \boldsymbol{x}_{2^S}] \quad (25)$$

We now observe that the slope of a deformed configuration is not dependent on the actual position of the origin of local coordinate system. So the only possibility to have independence is if

$$\boldsymbol{\mathcal{D}}^S \boldsymbol{S}^S \boldsymbol{I}^S_z \boldsymbol{E}^S \boldsymbol{x}_{2^S} = \boldsymbol{0} \quad (26)$$

Therefore, Eq. (25) is simplified as

$$\frac{\mathrm{d}\boldsymbol{\mathcal{Z}}^{S\text{step}\lambda\text{iter}n}_{\text{loc}}}{\mathrm{d}x^S} = \boldsymbol{\mathcal{D}}^S \boldsymbol{S}^S \boldsymbol{I}^S_z \boldsymbol{E}^S \boldsymbol{I}^S_d \boldsymbol{I}^S [\bar{\boldsymbol{x}}^{\text{step}\lambda\text{iter}n} + \boldsymbol{u}^{\text{step}\lambda\text{iter}n}] \quad (27)$$

Introducing the definition

$$\boldsymbol{a}^S_3 = \boldsymbol{S}^S \boldsymbol{I}^S_z \boldsymbol{E}^S \boldsymbol{I}^S_d \boldsymbol{I}^S \quad (28)$$

we get

$$\frac{\mathrm{d}\boldsymbol{\mathcal{Z}}^{S\text{step}\lambda\text{iter}n}_{\text{loc}}}{\mathrm{d}x^S} = \boldsymbol{\mathcal{D}}^S \boldsymbol{a}^S_3 [\bar{\boldsymbol{x}}^{\text{step}\lambda\text{iter}n} + \boldsymbol{u}^{\text{step}\lambda\text{iter}n}] \quad (29)$$

This formula relates the slope of all the control points of all panels of wing surface S to the augmented-coordinate vector at the beginning of the current iteration in the Newton–Raphson procedure. Also, the slopes are related to the unknown vector of displacements $\boldsymbol{u}^{\text{step}\lambda\text{iter}n}$. This last term will be used to generate the aerodynamic tangent matrix for the steady case. Equation (29) can be written for all wing segments and so an assembly procedure is required to have all the local slopes of all the panels of the entire wing system as a function of the augmented-coordinate vector and displacement vector of the full structural finite element model.

B. Unsteady Case (Doublet-Lattice Method)

When the unsteady case is considered, a known set of motion shapes is considered as generalized motions for unsteady

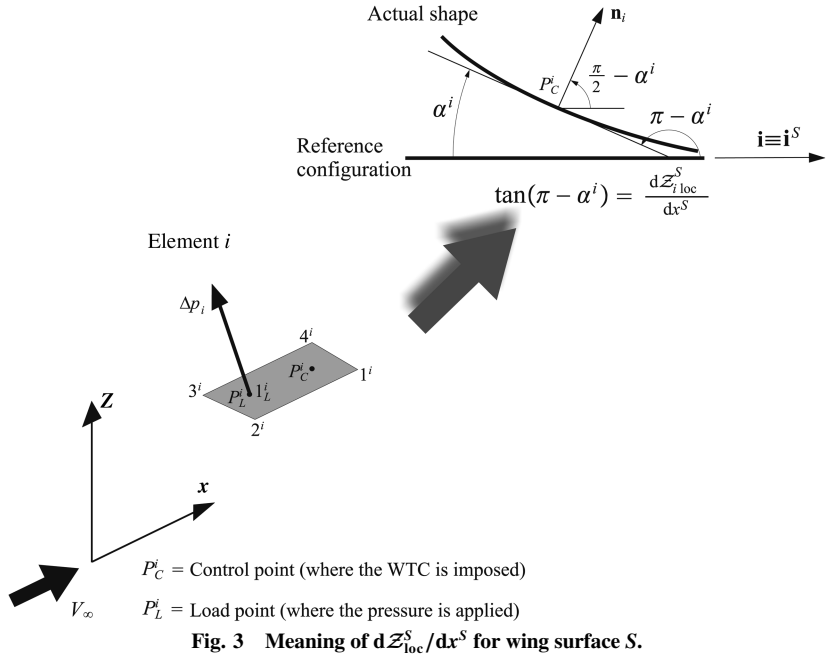

Fig. 3 Meaning of $\mathrm{d}\boldsymbol{\mathcal{Z}}^S_{\text{loc}}/\mathrm{d}x^S$ for wing surface S.

aerodynamic generalized force generation. Let $\boldsymbol{\Phi}_m$ be one generic shape of the set. The equivalent of Eq. (29) is

$$\frac{\mathrm{d}\boldsymbol{\mathcal{Z}}^S_{m\mathrm{loc}}}{\mathrm{d}x^S} = \boldsymbol{\mathcal{D}}^S \boldsymbol{a}^S_3[\bar{\boldsymbol{x}}^{\alpha=0} + \boldsymbol{\Phi}_m] \tag{30}$$

The generic shape $\boldsymbol{\Phi}_m$ is referred to the reference configuration. When $\boldsymbol{\Phi}_m = \boldsymbol{0}$, the reference configuration is obtained. Considering the fact that in the reference configuration we do not have slopes in the local coordinate system (there is no angle of attack), it can be deduced that $\boldsymbol{\mathcal{D}}^S \boldsymbol{a}^S_3 \bar{\boldsymbol{x}}^{\alpha=0} = \boldsymbol{0}$. Equation (30) is then

$$\frac{\mathrm{d}\boldsymbol{\mathcal{Z}}^S_{m\mathrm{loc}}}{\mathrm{d}x^S} = \boldsymbol{\mathcal{D}}^S \boldsymbol{a}^S_3 \boldsymbol{\Phi}_m \tag{31}$$

In the unsteady case, we also need the vector $\boldsymbol{\mathcal{Z}}^S_{m\mathrm{loc}}$, and not only its derivative given in Eq. (31), to impose the unsteady wall boundary conditions at the control points. Again using the splines, we can demonstrate the following formula:

$$\boldsymbol{\mathcal{Z}}^S_{m\mathrm{loc}} = \boldsymbol{\mathcal{D}}^{S\star} \boldsymbol{S}^S \boldsymbol{I}^S_z \cdot \boldsymbol{E}^S \cdot [\boldsymbol{I}^S_d \cdot \boldsymbol{I}^S \cdot \bar{\boldsymbol{x}}^{\alpha=0} + \boldsymbol{I}^S_d \cdot \boldsymbol{I}^S \cdot \boldsymbol{\Phi}_m - \boldsymbol{x}_{2^S}] \tag{32}$$

If the shape is exactly coincident with the reference configuration (i.e., $\boldsymbol{\Phi}_m = \boldsymbol{0}$), then the local z coordinates are exactly zeros. Thus, it can be deduced [see Eq. (32)] that

$$\boldsymbol{\mathcal{D}}^{S\star} \boldsymbol{S}^S \boldsymbol{I}^S_z \cdot \boldsymbol{E}^S \cdot [\boldsymbol{I}^S_d \cdot \boldsymbol{I}^S \cdot \bar{\boldsymbol{x}}^{\alpha=0} - \boldsymbol{x}_{2^S}] = \boldsymbol{0} \tag{33}$$

Using this finding, Eq. (32) is simplified as

$$\boldsymbol{\mathcal{Z}}^S_{m\mathrm{loc}} = \boldsymbol{\mathcal{D}}^{S\star} \boldsymbol{S}^S \boldsymbol{I}^S_z \cdot \boldsymbol{E}^S \cdot \boldsymbol{I}^S_d \cdot \boldsymbol{I}^S \cdot \boldsymbol{\Phi}_m \tag{34}$$

or

$$\boldsymbol{\mathcal{Z}}^S_{m\mathrm{loc}} = \boldsymbol{\mathcal{D}}^{S\star} \boldsymbol{a}^S_3 \cdot \boldsymbol{\Phi}_m \tag{35}$$

In the calculation of the generalized aerodynamic matrices, it is required to also transform loads at aerodynamic load points to nodes on the structural grid. Using a procedure formally identical to that used to obtain Eq. (35), it is possible to demonstrate that

$$\tilde{\boldsymbol{\mathcal{Z}}}^S_{m\mathrm{loc}} = \tilde{\boldsymbol{\mathcal{D}}}^{S\star} \boldsymbol{a}^S_3 \cdot \boldsymbol{\Phi}_m \tag{36}$$

where $\tilde{\boldsymbol{\mathcal{D}}}^{S\star}$ has a formal expression identical to $\boldsymbol{\mathcal{D}}^{S\star}$. The only difference is that the local coordinates of the load points are considered instead of the local coordinates of the control points.

C. Boundary Conditions Using the Doublet-Lattice Method

Under the assumption of simple harmonic motion, it is possible to demonstrate that the vector that contains the normalized (using the velocity V_∞) normal wash of all panels included in wing surface S has the following expression (the boundary condition is enforced on all control points of wing surface S):

$$\boldsymbol{w}^S_m = j\frac{\omega}{V_\infty}\boldsymbol{\mathcal{Z}}^S_{m\mathrm{loc}} + \frac{\partial \boldsymbol{\mathcal{Z}}^S_{m\mathrm{loc}}}{\partial x^S} = jk\boldsymbol{\mathcal{Z}}^S_{m\mathrm{loc}} + \frac{\partial \boldsymbol{\mathcal{Z}}^S_{m\mathrm{loc}}}{\partial x^S} \tag{37}$$

In the previous equation, all the vector quantities have to be understood as vectors of amplitudes of harmonic motion, where k is defined as the ratio ω/V_∞ (it is the reduced frequency $k^\star$ divided by the reference chord).

D. Assembling the Matrices Used for Mesh-to-Mesh Transformations

The aerodynamic panels are numbered to have the first N^1 panels of surface 1 and then the second N^2 panels of surface 2, and so forth. The assembly process is simple and all the prescribed values of the normal wash of all panels can be calculated and later equated to the values obtained by integrating the unsteady kernel. The assembly process is carried out by calculating all the products (for all wing segments) $\boldsymbol{\mathcal{D}}^S \boldsymbol{a}^S_3$, $\boldsymbol{\mathcal{D}}^{S\star} \boldsymbol{a}^S_3$, and $\tilde{\boldsymbol{\mathcal{D}}}^{S\star} \boldsymbol{a}^S_3$ and observing that each aerodynamic panel can be included in only one trapezoidal wing segment. This means that two different wing segments do not share aerodynamic panels.

After the assembly, at the wing-system level, Eqs. (29), (31), (35), and (36)[‡] are written as

$$\begin{aligned}
\frac{\mathrm{d}\boldsymbol{\mathcal{Z}}^{\mathrm{step}\lambda\mathrm{iter}n}_{\mathrm{loc}}}{\mathrm{d}x} &= \boldsymbol{A}_3[\bar{\boldsymbol{x}}^{\mathrm{step}\lambda\mathrm{iter}n} + \boldsymbol{u}^{\mathrm{step}\lambda\mathrm{iter}n}] \\
\frac{\mathrm{d}\boldsymbol{\mathcal{Z}}_{m\mathrm{loc}}}{\mathrm{d}x} &= \boldsymbol{A}_3 \cdot \boldsymbol{\Phi}_m \\
\boldsymbol{\mathcal{Z}}_{m\mathrm{loc}} &= \boldsymbol{A}^\star_3 \cdot \boldsymbol{\Phi}_m \\
\tilde{\boldsymbol{\mathcal{Z}}}_{m\mathrm{loc}} &= \tilde{\boldsymbol{A}}^\star_3 \cdot \boldsymbol{\Phi}_m
\end{aligned} \tag{38}$$

The vector that contains the normalized normal wash of all panels of all wing systems is

$$\boldsymbol{w}_m = jk\boldsymbol{\mathcal{Z}}_{m\mathrm{loc}} + \frac{\mathrm{d}\boldsymbol{\mathcal{Z}}_{m\mathrm{loc}}}{\mathrm{d}x} \tag{39}$$

VI. Full-Order Steady Aerodynamic Forces

When geometric nonlinearities are included, computation of the steady-state aeroelastic response has to be done incrementally. If a single aerodynamic-influence-coefficient matrix for aerodynamics corresponding to a constant Mach number is to be used, then this can be done by starting a reference configuration at a zero angle of attack and gradually increasing its angle of attack or by starting at a low dynamic pressure at constant Mach number and gradually increasing the dynamic pressure. Gradual increase of dynamic pressure at constant altitude by using a sequence of aerodynamic-influence-coefficient matrices at different Mach numbers is also possible.

Because of an initial focus on low-speed cases in this paper, aerodynamics at a Mach number of zero is assumed for all the load steps. At each load step, the pressure is incremented. At the final load step, the dynamic pressure will have reached its final value.

The formulation presented here covers both the vortex-lattice and doublet-lattice methods. A note on the DLM capability used here is in order. This capability integrates the unsteady kernel using Ueda's [13,37,51] formulas and a Gaussian quadrature formula. Because of this, it is not necessary to subtract the steady part of the kernel and use a vortex-lattice formulation for the steady case, as was done with the commonly used doublet-lattice codes [32].

The singularity of the kernel is handled by calculating the integrals analytically when the receiving panel is behind the sending panel along the same strip of aerodynamic panels. The DLM capability used here predicts the steady case well, with a formulation that is accurate for both zero and nonzero reduced frequencies. Comparison of results from the DLM capability used here and a conventional VLM capability confirms this.

In the steady case, considering that the structure changes configuration when it deforms, the boundary condition used for the doublet-lattice (DL) formulation is [see Eqs. (38) and (39)]

$$\boldsymbol{w}^{\mathrm{step}\lambda\mathrm{iter}n} = \frac{\mathrm{d}\boldsymbol{\mathcal{Z}}^{\mathrm{step}\lambda\mathrm{iter}n}_{\mathrm{loc}}}{\mathrm{d}x} = \boldsymbol{A}_3[\bar{\boldsymbol{x}}^{\mathrm{step}\lambda\mathrm{iter}n} + \boldsymbol{u}^{\mathrm{step}\lambda\mathrm{iter}n}] \tag{40}$$

where all the quantities are real numbers (steady case). The doublet-lattice key equation for the steady case is

$$\boldsymbol{w}^{\mathrm{step}\lambda\mathrm{iter}n} = \boldsymbol{A}^D \cdot \Delta\boldsymbol{p}^{\mathrm{step}\lambda\mathrm{iter}n} \tag{41}$$

where $\boldsymbol{A}^D$ is the aerodynamic-influence-coefficient matrix for the aerodynamic panels (this matrix is calculated once using the geometry of the aerodynamic reference configuration), and $\Delta\boldsymbol{p}^{\mathrm{step}\lambda\mathrm{iter}n}$ is a vector that contains all the dimensionless pressure loads on all aerodynamic panels.

For a generic panel, the aerodynamic force applied at the load point of that panel is obtained by multiplying a fraction of the dynamic pressure by some geometrical quantities of the panel and by

[‡]Equation (29) is used in the steady case only.

the dimensionless pressure load. (In the nonlinear steady analysis reported here, the load is not applied at once, and load steps correspond to a gradual increase in dynamic pressure.) Because this applies to all the wing-system segments, the vector that contains the scalar components of the aerodynamic forces of all the panels is written as a product between the fraction of the dynamic pressure and a matrix $\boldsymbol{I}_D$, which depends on the planform geometry. This matrix has to multiply the vector containing all the dimensionless pressure loads; thus,

$$\boldsymbol{L}^{\text{step}\lambda\text{iter}n} = \lambda L_{\text{ref}} \boldsymbol{I}_D \cdot \Delta \boldsymbol{p}^{\text{step}\lambda\text{iter}n} \tag{42}$$

where L_{ref} is the reference aerodynamic load. Its expression is

$$L_{\text{ref}} = \frac{\frac{1}{2}\rho_\infty V_\infty^2}{N_{\text{step}}} \tag{43}$$

where N_{step} is the number of load steps. From Eqs. (40) and (41), it is possible to relate the vector containing dimensionless pressures to the augmented-coordinate vector and displacement vector (the latter is unknown):

$$\Delta \boldsymbol{p}^{\text{step}\lambda\text{iter}n} = [\boldsymbol{A}^D]^{-1} \boldsymbol{w}^{\text{step}\lambda\text{iter}n} = [\boldsymbol{A}^D]^{-1} \boldsymbol{A}_3 [\bar{\boldsymbol{x}}^{\text{step}\lambda\text{iter}n} + \boldsymbol{u}^{\text{step}\lambda\text{iter}n}] \tag{44}$$

The vector with the aerodynamic forces [Eq. (42)] is then

$$\boldsymbol{L}^{\text{step}\lambda\text{iter}n} = \lambda L_{\text{ref}} \boldsymbol{I}_D \cdot [\boldsymbol{A}^D]^{-1} \boldsymbol{A}_3 [\bar{\boldsymbol{x}}^{\text{step}\lambda\text{iter}n} + \boldsymbol{u}^{\text{step}\lambda\text{iter}n}] \tag{45}$$

With the help of the definition

$$\bar{\boldsymbol{c}} \doteq \boldsymbol{I}_D [\boldsymbol{A}^D]^{-1} \boldsymbol{A}_3 \tag{46}$$

we obtain

$$\boldsymbol{L}^{\text{step}\lambda\text{iter}n} = \lambda L_{\text{ref}} \bar{\boldsymbol{c}} [\bar{\boldsymbol{x}}^{\text{step}\lambda\text{iter}n} + \boldsymbol{u}^{\text{step}\lambda\text{iter}n}] \tag{47}$$

The aerodynamic loads (forces) of Eq. (47) are applied at the load points of the aerodynamic panels. They are transferred to the structural nodes using the following procedure.

For all aerodynamic load points, the aerodynamic forces are extracted from Eq. (47). Then the triangular structural finite element that includes the load point of the generic aerodynamic panel is found. The equivalent loads applied at the nodes of the triangular FE element (which contains the load point) are obtained by using the area coordinates [58]. Finally, an assembly procedure is required (a node generally connects more FE elements). Note that some zero rows in correspondence of the rotational degrees of freedom have to be added. The vector of the aerodynamic forces applied at the structural nodes is written as

$$\boldsymbol{L}_{\text{str}}^{\text{step}\lambda\text{iter}n} = \lambda L_{\text{ref}} \boldsymbol{C} (\bar{\boldsymbol{x}}^{\text{step}\lambda\text{iter}n} + \boldsymbol{u}^{\text{step}\lambda\text{iter}n}) \tag{48}$$

where $\boldsymbol{C}$ is a constant matrix. Note also that $\boldsymbol{K}_{T\text{aero}}^{\text{step}\lambda} \doteq -\lambda L_{\text{ref}} \boldsymbol{C}$ is the *aerodynamic tangent matrix*.

It is convenient to write Eq. (48) in the form

$$\boldsymbol{L}_{\text{str}}^{\text{step}\lambda\text{iter}n} = \boldsymbol{L}_{\text{RHS}}^{\text{step}\lambda\text{iter}n} + \boldsymbol{L}_{\text{LHS}}^{\text{step}\lambda\text{iter}n} \tag{49}$$

where

$$\boldsymbol{L}_{\text{RHS}}^{\text{step}\lambda\text{iter}n} = \lambda L_{\text{ref}} \boldsymbol{C} \bar{\boldsymbol{x}}^{\text{step}\lambda\text{iter}n} \tag{50}$$

$$\boldsymbol{L}_{\text{LHS}}^{\text{step}\lambda\text{iter}n} = \lambda L_{\text{ref}} \boldsymbol{C} \boldsymbol{u}^{\text{step}\lambda\text{iter}n} = -\boldsymbol{K}_{\text{Taero}}^{\text{step}\lambda} \boldsymbol{u}^{\text{step}\lambda\text{iter}n} \tag{51}$$

The subscript LHS is used to point out that the term $\boldsymbol{L}_{\text{LHS}}^{\text{step}\lambda\text{iter}n}$ will go to the left-hand side of the equation iteratively solved in the Newton–Raphson procedure. If the vortex-lattice method is used, the final expression [Eq. (48)] is formally identical. In both DLM and VLM cases, the reference configuration is the one with no angle of attack. This, in theory, is not required by the VLM, but it is used to keep the same formalism valid for the DLM.

VII. Full-Order Steady Aerodynamic Forces Using the Concept of a Cumulative-Displacement Vector

The aerodynamic forces can be written in a different form using the concept of a cumulative-displacement vector. This equivalent writing is used in the dynamic case and is therefore introduced here. The steady aerodynamic loads can be written in a more elegant form by considering that when $\alpha = 0$ for all aerodynamic boxes, we do not have aerodynamic loads, and so we can write

$$\boldsymbol{L}_{\text{str}}^{\text{step}\lambda\text{iter}n} = \lambda L_{\text{ref}} (\boldsymbol{C} \bar{\boldsymbol{x}}^{\text{step}\lambda\text{iter}n} - \overbrace{\boldsymbol{C} \bar{\boldsymbol{x}}^{\alpha=0}}^{\text{This term is zero}} + \boldsymbol{C} \boldsymbol{u}^{\text{step}\lambda\text{iter}n}) \tag{52}$$

The coordinates at the *beginning* of the current iteration are the summation of all translational displacements that occurred in all the previous iterations and the coordinates of the nodes of the reference configuration. The product between the aerodynamic matrix $\boldsymbol{C}$ and the difference of the augmented-coordinate vector at the beginning of the current iteration and the augmented-coordinate vector at the reference configuration is equal to the product between the matrix $\boldsymbol{C}$ and the cumulative-displacement vector $\boldsymbol{U}^{\text{step}\lambda\text{iter}(n-1)}$ at the end of the previous iteration, because the local FE rotations at nodes do not influence the aerodynamic loads. The following relation is valid:

$$\bar{\boldsymbol{x}}^{\text{step}\lambda\text{iter}n} - \bar{\boldsymbol{x}}^{\alpha=0} \neq \boldsymbol{U}^{\text{step}\lambda\text{iter}(n-1)} \tag{53}$$

Because the FE rotations do not provide aerodynamic contribution, it can be concluded that

$$\boldsymbol{C}\, \bar{\boldsymbol{x}}^{\text{step}\lambda\text{iter}n} - \boldsymbol{C} \bar{\boldsymbol{x}}^{\alpha=0} = \boldsymbol{C} \boldsymbol{U}^{\text{step}\lambda\text{iter}(n-1)} \tag{54}$$

The aerodynamic loads can then be written as

$$\boldsymbol{L}_{\text{str}}^{\text{step}\lambda\text{iter}n} = \lambda L_{\text{ref}} (\boldsymbol{C} \boldsymbol{U}^{\text{step}\lambda\text{iter}(n-1)} + \boldsymbol{C} \boldsymbol{u}^{\text{step}\lambda\text{iter}n}) \tag{55}$$

which is a convenient form for application of the Newton–Raphson method. Note that at the end of a particular iteration, the cumulative-displacement vector is defined as the summation of all the displacements of the previous iterations and the displacement of the current iteration, and so the loads can be written in an even more compact form. This, however, is not convenient in practice, because we need to have a separate contribution in which the vector of the current displacements appears to identify the aerodynamic tangent matrix as the matrix that multiplies the unknown displacements:

$$\boldsymbol{L}_{\text{str}}^{\text{step}\lambda\text{iter}n} = \lambda L_{\text{ref}} \boldsymbol{C} \boldsymbol{U}^{\text{step}\lambda\text{iter}n} \tag{56}$$

where $\boldsymbol{U}^{\text{step}\lambda\text{iter}n}$ is the cumulative-displacement vector of the current iteration, and it is obtained as

$$\boldsymbol{U}^{\text{step}\lambda\text{iter}n} = \boldsymbol{U}^{\text{step}\lambda\text{iter}(n-1)} + \boldsymbol{u}^{\text{step}\lambda\text{iter}n} \tag{57}$$

A similar formula will be obtained in the dynamic case.

If the concept of cumulative displacement is used, then the right-hand side (RHS) of the aerodynamic loads is written as

$$\boldsymbol{L}_{\text{RHS}}^{\text{step}\lambda\text{iter}n} = \lambda L_{\text{ref}} \boldsymbol{C} \boldsymbol{U}^{\text{step}\lambda\text{iter}(n-1)} \tag{58}$$

VIII. Solution of the Nonlinear Steady-State Equations

Before the discussion of the Newton–Raphson solution procedure, some terminology should be introduced. We define the tangent matrix as the matrix that multiplies the unknown displacement vector. Because in our case we have the coupling of aerodynamic and structural mathematical models, we will have the aerodynamic tangent matrix and the structural tangent matrix. The summation of the two aforementioned matrices is the tangent matrix of the aeroelastic system.

The wing is loaded by external aerodynamic loads, motion-dependent aerodynamic loads, and other loads (indicated with $\boldsymbol{P}_{\text{ext}}$), such as the inertial loads. The Newton–Raphson solution procedure used proceeds as follows: the reference aerodynamic pressure L_{ref} is

first calculated, which is the increment in dynamic pressure from one load step to another:

$$L_{\text{ref}} = \frac{\frac{1}{2}\rho_\infty V_\infty^2}{N_{\text{step}}} \tag{59}$$

An increment of external concentrated loads can be similarly defined. The reference magnitude P_{ref} of those loads will be

$$P_{\text{ref}} = \frac{1}{N_{\text{step}}} \tag{60}$$

where P_{ref} is a dimensionless number.

Note that because aerodynamic influence coefficients are calculated for a configuration with zero angles of attack for all aerodynamic boxes and because this is the geometry from which motion starts, no motion-dependent aerodynamic loads appear initially, and unless there is a nonaerodynamic external load, the structure will not move. At the very first iteration of the Newton–Raphson procedure, an initial angle-of-attack perturbation is imposed:

$$\boldsymbol{x}^{\text{step1iter1}} = \boldsymbol{x}^{\text{pert}} \neq \boldsymbol{x}^{\alpha=0} \tag{61}$$

Considering this perturbation of the system, the cumulative-displacement vector is initialized [see Eq. (54)]:

$$\bar{\boldsymbol{x}}^{\text{step1iter1}} - \bar{\boldsymbol{x}}^{\alpha=0} = \boldsymbol{U}^0 \tag{62}$$

Mathematically, Eq. (62) is not correct [see Eq. (53)] and the RHS and left-hand side (LHS) of the equation are not equivalent. However, according to Eq. (54), when these quantities are multiplied by the aerodynamic matrix, then the equivalence is correct. So the initialization (62) can be done without introducing errors and with a great simplification of the theory.

The applied nonaerodynamic loads (of the nonfollower force type) are only step-dependent and they are calculated by using the following expression:

$$\boldsymbol{P}_{\text{str}}^{\text{step}\lambda} = \lambda \cdot P_{\text{ref}} \cdot \boldsymbol{P}_{\text{ext}} \tag{63}$$

The aerodynamic loads are calculated (at the very first iteration $\boldsymbol{U}^{\text{step}\lambda\text{iter}(n-1)} = \boldsymbol{U}^0$) as

$$\boldsymbol{L}_{\text{RHS}}^{\text{step}\lambda\text{iter}n} = \lambda L_{\text{ref}} \boldsymbol{C} \boldsymbol{U}^{\text{step}\lambda\text{iter}(n-1)} \tag{64}$$

where λ is the load factor, which is equal to 1 for the first load step, 2 for the second load step, and so forth. The internal forces $\boldsymbol{F}_{\text{int}}^{\text{step}\lambda\text{iter}n}$ are known from the previous iteration (if the very first iteration of the first load step is considered, there are no internal forces because the structure is initially assumed to be stress-free). So the unbalanced loads $\boldsymbol{P}_{\text{unb}}^{\text{step}\lambda\text{iter}n}$ can be calculated:

$$\boldsymbol{P}_{\text{unb}}^{\text{step}\lambda\text{iter}n} = \boldsymbol{P}_{\text{str}}^{\text{step}\lambda} + \boldsymbol{L}_{\text{RHS}}^{\text{step}\lambda\text{iter}n} - \boldsymbol{F}_{\text{int}}^{\text{step}\lambda\text{iter}n} \tag{65}$$

The structural tangent matrix $\boldsymbol{K}_T^{\text{step}\lambda\text{iter}n}$ is calculated by adding the elastic stiffness matrix $\boldsymbol{K}_E^{\text{step}\lambda\text{iter}n}$ (calculated considering the coordinates at the beginning of the nth iteration) and the geometric-stiffness matrix $\boldsymbol{K}_G^{\text{step}\lambda\text{iter}n}$. In practice, it is convenient to perform this operation at the element level and then assemble the resulting matrix:

$$\boldsymbol{K}_T^{\text{step}\lambda\text{iter}n} = \boldsymbol{K}_E^{\text{step}\lambda\text{iter}n} + \boldsymbol{K}_G^{\text{step}\lambda\text{iter}n} \tag{66}$$

The structural tangent matrix is updated at each iteration of the procedure. The term *iteration* used here refers to the repetitive refinement of a nonlinear solution for an incremental load step. It does not refer to the process of increasing loads and dynamic pressure incrementally.

The aerodynamic tangent matrix is calculated by

$$\boldsymbol{K}_{T\text{aero}}^{\text{step}\lambda} = -\lambda L_{\text{ref}} \boldsymbol{C} \tag{67}$$

Note that the aerodynamic tangent matrix is only load-step-dependent, because the matrix $\boldsymbol{C}$ is constant. The matrix is constant because of the linearity of the aerodynamic theory and the assumption that linearized aerodynamic loads calculated on a reference grid at the beginning of a load step will provide accurate aerodynamic loads for the process of converging at a load increment on the incremental-deformation solution. Because results are presented here for which dynamic pressure is increased incrementally, the procedure is valid when the flow can be considered incompressible or when dynamic pressure is increased at any other nonzero constant Mach number. If the Mach number is changed and the hypothesis of incompressible flow is removed, then the matrix $\boldsymbol{C}$ is not constant and it becomes load-step-dependent. In fact, when the convergence of a particular load step is reached, the load step is incremented by one and the dynamic pressure (and so the speed) is incremented as well. This increase means a different Mach number and so a different matrix $\boldsymbol{C}$ is calculated by the DL code. In this paper, this is not the case, and all the results will assume incompressible flow and constant aerodynamic matrix $\boldsymbol{C}$ calculated once.

Now the tangent matrix $\boldsymbol{K}_{\text{tangent}}^{\text{step}\lambda\text{iter}n}$ is built by adding the structural and aerodynamic tangent matrices as follows:

$$\boldsymbol{K}_{\text{tangent}}^{\text{step}\lambda\text{iter}n} = \boldsymbol{K}_T^{\text{step}\lambda\text{iter}n} + \boldsymbol{K}_{T\text{aero}}^{\text{step}\lambda} \tag{68}$$

The following linear system can now be solved, and the displacement vector $\boldsymbol{u}^{\text{step}\lambda\text{iter}n}$ can be found:

$$\boldsymbol{K}_{\text{tangent}}^{\text{step}\lambda\text{iter}n} \cdot \boldsymbol{u}^{\text{step}\lambda\text{iter}n} = \boldsymbol{P}_{\text{unb}}^{\text{step}\lambda\text{iter}n} \tag{69}$$

Node-location coordinates are updated for the next iteration:

$$\boldsymbol{x}^{\text{step}\lambda\text{iter}(n+1)} = \boldsymbol{x}^{\text{step}\lambda\text{iter}n} + \boldsymbol{u}_d^{\text{step}\lambda\text{iter}n} \tag{70}$$

where $\boldsymbol{u}_d^{\text{step}\lambda,\text{iter}n}$ is the vector that contains only the translational degrees of freedom, and it is obtained from the vector of displacements $\boldsymbol{u}^{\text{step}\lambda,\text{iter}n}$ by eliminating the rows corresponding to the rotations. If the last iteration of the load step λ has been performed, then the left-hand side of the previous equation is $\boldsymbol{x}^{\text{step}(\lambda+1)\text{iter}1}$ instead of $\boldsymbol{x}^{\text{step}\lambda\text{iter}(n+1)}$.

Rigid-body motion is eliminated from elements according to the Gal–Levy [47] procedure, and the pure elastic rotations and strains are found. Using these quantities, the internal forces are updated for the next iteration and therefore the vector $\boldsymbol{F}_{\text{int}}^{\text{step}\lambda\text{iter}(n+1)}$ is created. (In the case in which the last iteration of load step λ has been performed, the term $\boldsymbol{F}_{\text{int}}^{\text{step}\lambda\text{iter}(n+1)}$ has to be replaced by $\boldsymbol{F}_{\text{int}}^{\text{step}(\lambda+1)\text{iter}1}$.)

The cumulative-displacement vector is updated next:

$$\boldsymbol{U}^{\text{step}\lambda\text{iter}n} = \boldsymbol{U}^{\text{step}\lambda\text{iter}(n-1)} + \boldsymbol{u}^{\text{step}\lambda\text{iter}n} \tag{71}$$

The procedure is repeated until a desired convergence tolerance is reached.

IX. Steady Aeroelastic Case: Full-Order Structural Model and Modally-Reduced-Order Aerodynamic Model

A. Approximated Aerodynamic Tangent Matrix Obtained from the Generalized Aerodynamic Tangent Matrix

Order reduction of the structural system by using a known set of deformation-shape vectors (which can be, for example, the natural modes of the structure or other sets of assigned shapes) is a major challenge when geometrical nonlinearities are considered. For example, in the joined-wing configuration, in-plane forces in the rear wing and the inner section of the main wing are important in the calculation of the geometric-stiffness matrix. A modal basis has to be able to capture stress distributions as well as deformation shapes. The fact that the nodes are moving and can move significantly also adds difficulty. The conventional modal approach, so widespread in linear aeroelasticity, does not work with joined wings. As a matter of fact, it has already been shown that a basis built by adopting this procedure

leads to poor results unless the basis is continuously updated, leading to expensive computation [43]. Advanced procedures, such as the use of modes and modal derivatives, improve the approximation, but also tend to fail when joined wings are concerned.

The approach proposed in this paper is to use the full-order structural matrices to capture the nonlinear structural behavior and a modally reduced aerodynamic matrix calculated, for example, by adopting a commercial code such as ZAERO or another package. In this paper, a dedicated DLM code is used. When dynamic aeroelastic cases are considered, the proposed approach is particularly attractive because it allows the use of existing standard unsteady aerodynamic codes.

Consider a set $\boldsymbol{\Psi}$ of $\Re$ known shape vectors:

$$\boldsymbol{\Psi} = [\,\boldsymbol{\Phi}_1 \quad \boldsymbol{\Phi}_2 \quad \boldsymbol{\Phi}_3 \quad \cdots \quad \boldsymbol{\Phi}_{\Re}\,] \tag{72}$$

Let $\boldsymbol{\mathcal{A}}_0$ be the generalized aerodynamic matrix calculated for the steady case, and so $k^\star = 0$, where $k^\star$ is the reduced frequency obtained by using a commercial code using the basis $\boldsymbol{\Psi}$. The matrix $\boldsymbol{\mathcal{A}}_0$ has the dimensions $\Re \times \Re$. The generalized aerodynamic tangent matrix $\boldsymbol{\mathcal{A}}_Z$ is defined by multiplying $\boldsymbol{\mathcal{A}}_0$ by the fraction of the aerodynamic pressure related to the current load step λ. We use the negative sign to have an expression on the LHS of the equilibrium equation without negative signs:

$$\boldsymbol{\mathcal{A}}_Z \doteq -\lambda \cdot \frac{\frac{1}{2}\rho_\infty V_\infty^2}{N_{\text{step}}}\boldsymbol{\mathcal{A}}_0 = -\lambda \cdot L_{\text{ref}}\boldsymbol{\mathcal{A}}_0 \tag{73}$$

Suppose we approximate the displacements of iteration n of load step λ by using the basis $\boldsymbol{\Psi}$ and the vector $\boldsymbol{q}^{\text{step}\lambda\text{iter}n}$ of generalized coordinates as follows:

$$\boldsymbol{u}^{\text{step}\lambda\text{iter}n} \approx [\,\boldsymbol{\Phi}_1 \quad \boldsymbol{\Phi}_2 \quad \boldsymbol{\Phi}_3 \quad \cdots \quad \boldsymbol{\Phi}_{\Re}\,]\begin{bmatrix} q_1^{\text{step}\lambda\text{iter}n} \\ q_2^{\text{step}\lambda\text{iter}n} \\ q_3^{\text{step}\lambda\text{iter}n} \\ \cdots \\ q_{\Re}^{\text{step}\lambda\text{iter}n} \end{bmatrix} = \boldsymbol{\Psi}\boldsymbol{q}^{\text{step}\lambda\text{iter}n} \tag{74}$$

By applying the least-squares method (LSM), it is possible to express the generalized displacements as functions of the full-order displacements. But the finite element degrees of freedom include nodal rotations, which are usually not used in the interpolation of displacement and angle of attack over lifting surfaces for aeroelastic applications. The least-squares approximation should focus on matching the modal approximation to the full-order displaced shape of lifting-surface panels. The relation of full-order displacements to generalized displacements is represented by Eq. (74). Note that $\boldsymbol{u}^{\text{step}\lambda\text{iter}n}$ includes the rotations. By eliminating the rows that correspond to the rotations, the translational displacements $\boldsymbol{u}_d^{\text{step}\lambda\text{iter}n}$ are found as

$$\boldsymbol{u}_d^{\text{step}\lambda\text{iter}n} = \boldsymbol{\Psi}_d\boldsymbol{q}^{\text{step}\lambda\text{iter}n} \tag{75}$$

where $\boldsymbol{\Psi}_d$ contains only translational components of the $\Re$ shape vectors of the basis $\boldsymbol{\Psi}$. The dimension of $\boldsymbol{\Psi}_d$ is then $3N_n \times \Re$:

$$\boldsymbol{u}_d^{\text{step}\lambda\text{iter}n} = \boldsymbol{\Psi}_d\boldsymbol{q}^{\text{step}\lambda\text{iter}n} \Rightarrow \boldsymbol{\Psi}_d^T\boldsymbol{u}_d^{\text{step}\lambda\text{iter}n} = \boldsymbol{\Psi}_d^T\boldsymbol{\Psi}_d\boldsymbol{q}^{\text{step}\lambda\text{iter}n} \tag{76}$$

$$\boldsymbol{q}^{\text{step}\lambda\text{iter}n} = \left[\,\boldsymbol{\Psi}_d^T \quad \boldsymbol{\Psi}_d\,\right]^{-1}\boldsymbol{\Psi}_d^T\boldsymbol{u}_d^{\text{step}\lambda\text{iter}n} = \boldsymbol{T}_d\boldsymbol{u}_d^{\text{step}\lambda\text{iter}n} \tag{77}$$

where

$$\boldsymbol{T}_d = \left[\,\boldsymbol{\Psi}_d^T \quad \boldsymbol{\Psi}_d\,\right]^{-1}\boldsymbol{\Psi}_d^T \tag{78}$$

where $\boldsymbol{T}_d$ is a matrix with the dimensions $\Re \times 3N_n$. Another possibility is to perform the LSM fit only on the component of the displacements perpendicular to the surfaces. In the case of the delta wing of [22,23], the wing is contained in the x–y plane. Therefore, the displacement perpendicular to the surfaces is the displacement u_z. So the LSM fit can be performed only on the translational displacement u_z of all nodes. If this approach is chosen, the matrix $\boldsymbol{T}_d$ has the dimensions $\Re \times N_n$ (instead of $\Re \times 3N_n$), the matrix $\boldsymbol{\Psi}_d$ has the dimensions $N_n \times \Re$ (instead of $3N_n \times \Re$), and the vector $\boldsymbol{u}_d^{\text{step}\lambda\text{iter}n}$ contains just N_n elements (instead of $3N_n$).

It is preferable to work with the vector $\boldsymbol{u}^{\text{step}\lambda\text{iter}n}$ instead of the vector $\boldsymbol{u}_d^{\text{step}\lambda\text{iter}n}$. Therefore, columns of zeros in correspondence to the finite element nodal rotations (and the displacements u_x and u_y in the case in which the LSM fit is performed on the component u_z only) in matrix $\boldsymbol{T}_d$ are added. $\boldsymbol{T}$ is defined as the matrix $\boldsymbol{T}_d$ after the columns are added. The dimensions of this matrix are $\Re \times 6N_n$. Considering this new matrix, an equivalent writing of Eq. (77) that uses all degrees of freedom (DOF) is as follows:

$$\boldsymbol{q}^{\text{step}\lambda\text{iter}n} = \boldsymbol{T}\boldsymbol{u}^{\text{step}\lambda\text{iter}n} \tag{79}$$

Now the generalized aerodynamic tangent matrix has to be converted to correspond to the full-order structural model. This is achieved by imposing work/energy conservation.

The generalized forces are [the negative sign is a consequence of the negative sign used in Eq. (73)]

$$\boldsymbol{Q}^{\text{step}\lambda\text{iter}n} = -\boldsymbol{\mathcal{A}}_Z\boldsymbol{q}^{\text{step}\lambda\text{iter}n} = +\lambda \cdot L_{\text{ref}}\boldsymbol{\mathcal{A}}_0\boldsymbol{q}^{\text{step}\lambda\text{iter}n} \tag{80}$$

The work done by the generalized aerodynamic forces is

$$\delta W = \delta[\boldsymbol{q}^{\text{step}\lambda\text{iter}n}]^T \cdot \boldsymbol{Q}^{\text{step}\lambda\text{iter}n} \tag{81}$$

The work done by the equivalent aerodynamic forces $\boldsymbol{L}_{\text{LHS}}^{\text{step}\lambda\text{iter}n}$ applied on the structural mesh is

$$\delta W = \delta[\boldsymbol{u}^{\text{step}\lambda\text{iter}n}]^T \cdot \boldsymbol{L}_{\text{LHS}}^{\text{step}\lambda\text{iter}n} \tag{82}$$

Using Eq. (79) and equating Eqs. (81) and (82), it is possible to write

$$\delta[\boldsymbol{u}^{\text{step}\lambda\text{iter}n}]^T \cdot \boldsymbol{L}_{\text{LHS}}^{\text{step}\lambda\text{iter}n} = \delta[\boldsymbol{q}^{\text{step}\lambda\text{iter}n}]^T \cdot \boldsymbol{Q}^{\text{step}\lambda\text{iter}n} \tag{83}$$

From which it follows that

$$\boldsymbol{L}_{\text{LHS}}^{\text{step}\lambda\text{iter}n} = \boldsymbol{T}^T \cdot \boldsymbol{Q}^{\text{step}\lambda\text{iter}n} \tag{84}$$

Using Eqs. (79) and (80),

$$\boldsymbol{L}_{\text{LHS}}^{\text{step}\lambda\text{iter}n} = +\lambda L_{\text{ref}}\boldsymbol{T}^T\boldsymbol{\mathcal{A}}_0\boldsymbol{q}^{\text{step}\lambda\text{iter}n} = +\lambda L_{\text{ref}}\boldsymbol{T}^T\boldsymbol{\mathcal{A}}_0\boldsymbol{T}\boldsymbol{u}^{\text{step}\lambda\text{iter}n} \tag{85}$$

To keep the formalism used when the aerodynamic tangent matrix was obtained using the doublet-lattice formulation, we indicate the approximated aerodynamic tangent matrix with $\boldsymbol{K}_{T\text{Zaero}}^{\text{step}\lambda}$. The following definition is also made:

$$\boldsymbol{K}_{T\text{Zaero}}^{\text{step}\lambda} \doteq -\lambda \cdot L_{\text{ref}}\boldsymbol{C}_Z \tag{86}$$

where $\boldsymbol{C}_Z$ is the approximated counterpart of the matrix $\boldsymbol{C}$ defined earlier.

Equation (85) is then rewritten as [also see the analog Eq. (67) for the full-order exact case]

$$\boldsymbol{L}_{\text{LHS}}^{\text{step}\lambda\text{iter}n} = -\boldsymbol{K}_{T\text{Zaero}}^{\text{step}\lambda}\boldsymbol{u}^{\text{step}\lambda\text{iter}n} = +\lambda L_{\text{ref}}\boldsymbol{C}_Z\boldsymbol{u}^{\text{step}\lambda\text{iter}n} \tag{87}$$

Using Eq. (85), it can be deduced that

$$\boldsymbol{C}_Z = +\boldsymbol{T}^T\boldsymbol{\mathcal{A}}_0\boldsymbol{T} \tag{88}$$

where $\boldsymbol{K}_{T\text{Zaero}}^{\text{step}\lambda} = -\lambda L_{\text{ref}}\boldsymbol{C}_Z$ is the approximated aerodynamic tangent matrix obtained by using the generalized aerodynamic matrix $\boldsymbol{\mathcal{A}}_0$ calculated with the aerodynamic commercial code.

X. Unsteady Case: Time-Domain Simulations with Full-Order Structural Model and Reduced-Order Aerodynamic Model

The Fourier transform of the unsteady aerodynamic force [60] corresponding to the full-order structural finite element model is

$$\boldsymbol{L}_{\text{unsteady}}(j\omega) = \tfrac{1}{2}\rho_\infty V_\infty^2 \boldsymbol{\mathcal{A}}_{\text{full}}(j\omega)\cdot[\bar{\boldsymbol{x}} - \bar{\boldsymbol{x}}^{\alpha=0}](j\omega) \tag{89}$$

where $\bar{\boldsymbol{x}}$ is the augmented-coordinate vector (that is, the vector of nodal motions with rotational nodal motions zeroed out) and $\bar{\boldsymbol{x}}^{\alpha=0}$ is the vector of initial nodal coordinates corresponding to the condition of a zero angle of attack on all aerodynamic boxes (rotational nodal motions are removed as well). The difference $\bar{\boldsymbol{x}} - \bar{\boldsymbol{x}}^{\alpha=0}$ is a function of $j\omega$ because of the time dependence of nodal positions. For the unsteady case, we use the same transformation from generalized coordinates to full-order finite element coordinates as in the steady case using the same transformation matrix $\boldsymbol{T}$. We have

$$\boldsymbol{\mathcal{A}}_{\text{full}}(j\omega) = \boldsymbol{T}^T \boldsymbol{\mathcal{A}}(j\omega)\boldsymbol{T} \tag{90}$$

The matrix $\boldsymbol{\mathcal{A}}(j\omega)$ generated by an unsteady aerodynamic linear potential code is a nonrational function of the reduced frequency $k^\star = (\omega b/V_\infty)$: $\boldsymbol{\mathcal{A}} = \boldsymbol{\mathcal{A}}(jk^\star)$. In the present DL code, the reduced frequency was calculated based on a reference semichord of 1: that is, as $k = \omega/V_\infty$. A Roger procedure [61,62] is used to obtain a rational function approximation of the generalized unsteady loads. In particular,

$$\boldsymbol{\mathcal{A}}(jk^\star) = \boldsymbol{\mathcal{A}}_0 + (jk^\star)\boldsymbol{\mathcal{A}}_1 + (jk^\star)^2\boldsymbol{\mathcal{A}}_2 + \sum_{i=1}^{N_{\text{lag}}} \frac{jk^\star}{jk^\star + \beta_i}\boldsymbol{\mathcal{A}}_{2+i} \tag{91}$$

Recalling the definition of reduced frequency $k^\star = \omega b/V_\infty$, defining $\bar{\beta}_i = (V_\infty/b)\beta_i$, simplifying, and using analytical continuation to expand from the imaginary axis to the Laplace domain adjacent to it $j\omega \to s$, it is possible to write the aerodynamic generalized matrix in the Laplace domain, for which s is the Laplace variable:

$$\boldsymbol{\mathcal{A}}_2(s) = \boldsymbol{\mathcal{A}}_0 + s\frac{b}{V_\infty}\boldsymbol{\mathcal{A}}_1 + s^2\frac{b^2}{V_\infty^2}\boldsymbol{\mathcal{A}}_2 + \sum_{i=1}^{N_{\text{lag}}} \frac{s}{s+\bar{\beta}_i}\boldsymbol{\mathcal{A}}_{2+i} \tag{92}$$

The aerodynamic-force vector in the Laplace domain is

$$\boldsymbol{L}_{\text{unsteady}}(s) = \frac{1}{2}\rho_\infty V_\infty^2 \boldsymbol{T}^T\left[\boldsymbol{\mathcal{A}}_0 + s\frac{b}{V_\infty}\boldsymbol{\mathcal{A}}_1 + s^2\frac{b^2}{V_\infty^2}\boldsymbol{\mathcal{A}}_2 + \sum_{i=1}^{N_{\text{lag}}}\frac{s}{s+\bar{\beta}_i}\boldsymbol{\mathcal{A}}_{2+i}\right]\boldsymbol{T}[\bar{\boldsymbol{x}} - \bar{\boldsymbol{x}}^{\alpha=0}](s) \tag{93}$$

The following definitions are now introduced:

$$\begin{aligned} &\boldsymbol{\mathcal{A}}_0^\star \doteq \tfrac{1}{2}\rho_\infty V_\infty^2 \boldsymbol{T}^T\boldsymbol{\mathcal{A}}_0\boldsymbol{T}; \qquad \boldsymbol{\mathcal{A}}_1^\star \doteq \tfrac{1}{2}\rho_\infty b V_\infty \boldsymbol{T}^T\boldsymbol{\mathcal{A}}_1\boldsymbol{T} \\ &\boldsymbol{\mathcal{A}}_2^\star \doteq \tfrac{1}{2}\rho_\infty b^2 \boldsymbol{T}^T\boldsymbol{\mathcal{A}}_2\boldsymbol{T}; \qquad \boldsymbol{\mathcal{A}}_{2+i}^\star \doteq \tfrac{1}{2}\rho_\infty V_\infty^2 \boldsymbol{T}^T\boldsymbol{\mathcal{A}}_{2+i}\boldsymbol{T} \\ &i = 1, N_{\text{lag}} \end{aligned} \tag{94}$$

The unsteady aerodynamic forces in the Laplace domain can now be expressed as

$$\boldsymbol{L}_{\text{unsteady}}(s) = \left[\boldsymbol{\mathcal{A}}_0^\star + s\boldsymbol{\mathcal{A}}_1^\star + s^2\boldsymbol{\mathcal{A}}_2^\star + \sum_{i=1}^{N_{\text{lag}}}\frac{s}{s+\bar{\beta}_i}\boldsymbol{\mathcal{A}}_{2+i}^\star\right] \times [\bar{\boldsymbol{x}} - \bar{\boldsymbol{x}}^{\alpha=0}](s) \tag{95}$$

Using the inverse Laplace transform (ILT) [63] expressions in the time domain can be obtained. We can write

$$\begin{aligned} &\mathcal{L}^{-1}[\boldsymbol{\mathcal{A}}_0^\star \cdot [\bar{\boldsymbol{x}} - \bar{\boldsymbol{x}}^{\alpha=0}](s)] = \boldsymbol{\mathcal{A}}_0^\star \cdot [\bar{\boldsymbol{x}} - \bar{\boldsymbol{x}}^{\alpha=0}](t) \\ &\mathcal{L}^{-1}[s\boldsymbol{\mathcal{A}}_1^\star \cdot [\bar{\boldsymbol{x}} - \bar{\boldsymbol{x}}^{\alpha=0}](s)] = \boldsymbol{\mathcal{A}}_1^\star \cdot \frac{\mathrm{d}}{\mathrm{d}t}[\bar{\boldsymbol{x}} - \bar{\boldsymbol{x}}^{\alpha=0}](t) \\ &\mathcal{L}^{-1}[s^2\boldsymbol{\mathcal{A}}_2^\star \cdot [\bar{\boldsymbol{x}} - \bar{\boldsymbol{x}}^{\alpha=0}](s)] = \boldsymbol{\mathcal{A}}_2^\star \cdot \frac{\mathrm{d}^2}{\mathrm{d}t^2}[\bar{\boldsymbol{x}} - \bar{\boldsymbol{x}}^{\alpha=0}](t) \end{aligned} \tag{96}$$

The previous equations are valid if at $t = 0$, displacements, speeds, and accelerations are all zero. To transform the lag terms to the time domain, convolution integrals are used [62]. Using the Dirac delta function $\delta(t)$, the ILT of the term $s/(s+\bar{\beta}_i)$ is

$$\mathcal{L}^{-1}\left[\frac{s}{s+\bar{\beta}_i}\right] = \delta(t) - \bar{\beta}_i e^{-\bar{\beta}_i t} \tag{97}$$

Then, by applying the convolution theorem, we have

$$\begin{aligned} \mathcal{L}^{-1}\left[\frac{s}{s+\bar{\beta}_i}\boldsymbol{\mathcal{A}}_{2+i}^\star \cdot [\bar{\boldsymbol{x}} - \bar{\boldsymbol{x}}^{\alpha=0}](s)\right] &= \int_0^t [\delta(t-\tau) \\ &- \bar{\beta}_i e^{-\bar{\beta}_i(t-\tau)}]\boldsymbol{\mathcal{A}}_{2+i}^\star \cdot [\bar{\boldsymbol{x}} - \bar{\boldsymbol{x}}^{\alpha=0}](\tau)\,\mathrm{d}\tau \end{aligned} \tag{98}$$

or

$$\begin{aligned} \mathcal{L}^{-1}\left[\frac{s}{s+\bar{\beta}_i}\boldsymbol{\mathcal{A}}_{2+i}^\star \cdot [\bar{\boldsymbol{x}} - \bar{\boldsymbol{x}}^{\alpha=0}](s)\right] &= \boldsymbol{\mathcal{A}}_{2+i}^\star \cdot [\bar{\boldsymbol{x}} - \bar{\boldsymbol{x}}^{\alpha=0}](t) \\ &- \bar{\beta}_i \boldsymbol{\mathcal{A}}_{2+i}^\star \int_0^t [\bar{\boldsymbol{x}} - \bar{\boldsymbol{x}}^{\alpha=0}](\tau) e^{-\bar{\beta}_i(t-\tau)}\,\mathrm{d}\tau \end{aligned} \tag{99}$$

Using these inverse Laplace transform equations (96) and (99), the unsteady aerodynamic loads in the time domain become

$$\begin{aligned} \boldsymbol{L}_{\text{unsteady}}(t) &= \boldsymbol{\mathcal{A}}^\star[\bar{\boldsymbol{x}} - \bar{\boldsymbol{x}}^{\alpha=0}](t) + \boldsymbol{\mathcal{A}}_1^\star \cdot \frac{\mathrm{d}}{\mathrm{d}t}[\bar{\boldsymbol{x}} - \bar{\boldsymbol{x}}^{\alpha=0}](t) + \boldsymbol{\mathcal{A}}_2^\star \\ &\cdot \frac{\mathrm{d}^2}{\mathrm{d}t^2}[\bar{\boldsymbol{x}} - \bar{\boldsymbol{x}}^{\alpha=0}](t) - \sum_{i=1}^{N_{\text{lag}}} \bar{\beta}_i \boldsymbol{\mathcal{A}}_{2+i}^\star \int_0^t [\bar{\boldsymbol{x}} - \bar{\boldsymbol{x}}^{\alpha=0}](\tau) e^{-\bar{\beta}_i(t-\tau)}\,\mathrm{d}\tau \end{aligned} \tag{100}$$

where

$$\boldsymbol{\mathcal{A}}^\star \doteq \boldsymbol{\mathcal{A}}_0^\star + \sum_{i=1}^{N_{\text{lag}}} \boldsymbol{\mathcal{A}}_{2+i}^\star \tag{101}$$

As for the steady case, in general, $\boldsymbol{U} \neq \bar{\boldsymbol{x}} - \bar{\boldsymbol{x}}^{\alpha=0}$. But because structural rotational motions at nodes do not affect the unsteady aerodynamic loads in our formulation (slopes obtained from interpolated deformation shapes do), it is possible to replace the quantity $\bar{\boldsymbol{x}} - \bar{\boldsymbol{x}}^{\alpha=0}$ with the cumulative-displacement vector $\boldsymbol{U}$. The following definitions are now introduced:

$$\begin{aligned} &\boldsymbol{U}(t) \doteq {}^t\boldsymbol{U}; \qquad {}^t\dot{\boldsymbol{U}} \doteq \frac{\mathrm{d}[\boldsymbol{U}(t)]}{\mathrm{d}t}; \qquad {}^t\ddot{\boldsymbol{U}} \doteq \frac{\mathrm{d}^2[\boldsymbol{U}(t)]}{\mathrm{d}t^2} \\ &{}^t\boldsymbol{L}_{\text{unsteady}} \doteq \boldsymbol{L}_{\text{unsteady}}(t) \end{aligned} \tag{102}$$

The time-domain aerodynamic forces will have the expression [see Eq. (100)]

$$\begin{aligned} {}^t\boldsymbol{L}_{\text{unsteady}} &= \boldsymbol{\mathcal{A}}^\star \cdot {}^t\boldsymbol{U} + \boldsymbol{\mathcal{A}}_1^\star \cdot {}^t\dot{\boldsymbol{U}} + \boldsymbol{\mathcal{A}}_2^\star \cdot {}^t\ddot{\boldsymbol{U}} \\ &- \sum_{i=1}^{N_{\text{lag}}} \bar{\beta}_i \boldsymbol{\mathcal{A}}_{2+i}^\star \int_0^t {}^\tau\boldsymbol{U} e^{-\bar{\beta}_i(t-\tau)}\,\mathrm{d}\tau \end{aligned} \tag{103}$$

The expression of the aerodynamic loads [Eq. (103)] also covers the steady case [Eq. (56)]: to demonstrate that, consider Eq. (103). In the steady case, there is no time dependency and no contributions of aerodynamic-lag terms. Aerodynamic pressure loads are applied gradually and load steps are required. The steady counterpart of Eq. (103) is therefore

$$\boldsymbol{L}_{\text{str}}^{\text{step}\lambda\text{iter}n} = \boldsymbol{\mathcal{A}}_0^{\star\text{step}\lambda} \cdot \boldsymbol{U}^{\text{step}\lambda\text{iter}n} \tag{104}$$

The definition of the matrix $\mathcal{A}_0^{\star\text{step}\lambda}$ is [see Eq. (94)]

$$\mathcal{A}_0^{\star\text{step}\lambda} = \frac{\lambda}{N_{\text{step}}}\frac{1}{2}\rho_\infty V_\infty^2 \boldsymbol{T}^T \mathcal{A}_0 \boldsymbol{T} = \lambda L_{\text{ref}} \boldsymbol{T}^T \mathcal{A}_0 \boldsymbol{T} \tag{105}$$

Using Eq. (88),

$$\mathcal{A}_0^{\star\text{step}\lambda} = \lambda L_{\text{ref}} \boldsymbol{C}_Z \tag{106}$$

Substitution of this result into Eq. (104) leads to

$$\boldsymbol{L}_{\text{str}}^{\text{step}\lambda\text{iter}n} = \lambda L_{\text{ref}} \boldsymbol{C}_Z \cdot \boldsymbol{U}^{\text{step}\lambda\text{iter}n} \tag{107}$$

which is the approximated counterpart of Eq. (56). The procedure used here to approximate the unsteady aerodynamic loads thus leads to the procedure used to approximate the aerodynamic loads in the steady case and is consistent with it.

XI. Newmark's Method

Newmark's method [58] can be expressed using the following equations (Δt is the time step):

$${}^{t+\Delta t}\dot{\boldsymbol{U}} = {}^{t}\dot{\boldsymbol{U}} + [(1-\delta)\,{}^{t}\ddot{\boldsymbol{U}} + \delta\,{}^{t+\Delta t}\ddot{\boldsymbol{U}}]\Delta t \tag{108}$$

$${}^{t+\Delta t}\boldsymbol{U} = {}^{t}\boldsymbol{U} + {}^{t}\dot{\boldsymbol{U}}\Delta t + [(\tfrac{1}{2}-\alpha)\,{}^{t}\ddot{\boldsymbol{U}} + \alpha\,{}^{t+\Delta t}\ddot{\boldsymbol{U}}]\Delta t^2 \tag{109}$$

Then

$${}^{t+\Delta t}\ddot{\boldsymbol{U}} = \frac{1}{\alpha\Delta t^2}({}^{t+\Delta t}\boldsymbol{U} - {}^{t}\boldsymbol{U}) - \frac{1}{\alpha\Delta t}{}^{t}\dot{\boldsymbol{U}} - \left(\frac{1}{2\alpha}-1\right){}^{t}\ddot{\boldsymbol{U}} \tag{110}$$

The values $\delta = \frac{1}{2}$ and $\alpha = \frac{1}{4}$ are used here. In this case, the symbol δ does not represent the Dirac delta function but a parameter used in Newmark's method. Define

$$\begin{aligned} &a_0 = \frac{1}{\alpha(\Delta t)^2} \qquad a_1 = \frac{\delta}{\alpha\Delta t} \qquad a_2 = \frac{1}{\alpha\Delta t} \qquad a_3 = \frac{1}{2\alpha} - 1 \\ &a_4 = \frac{\delta}{\alpha} - 1 \qquad a_5 = \frac{\Delta t}{2}\left(\frac{\delta}{\alpha} - 2\right) \qquad a_6 = \Delta t(1-\delta) \\ &a_7 = \delta\Delta t \end{aligned} \tag{111}$$

Now acceleration and velocity vectors become

$${}^{t+\Delta t}\ddot{\boldsymbol{U}} = a_0({}^{t+\Delta t}\boldsymbol{U} - {}^{t}\boldsymbol{U}) - a_2{}^{t}\dot{\boldsymbol{U}} - a_3{}^{t}\ddot{\boldsymbol{U}} \tag{112}$$

$${}^{t+\Delta t}\dot{\boldsymbol{U}} = {}^{t}\dot{\boldsymbol{U}} + a_6{}^{t}\ddot{\boldsymbol{U}} + a_7{}^{t+\Delta t}\ddot{\boldsymbol{U}} \tag{113}$$

XII. Newmark's Time-Integration Unsteady Newton–Raphson Method for the Case of Mechanical Loads

The equation that has to be solved at each iteration is

$$\boldsymbol{M} \cdot {}^{t+\Delta t}\ddot{\boldsymbol{U}}^n + \boldsymbol{C}_D \cdot {}^{t+\Delta t}\dot{\boldsymbol{U}}^n + {}^{t+\Delta t}\boldsymbol{K}_T^n \cdot {}^{t+\Delta t}\boldsymbol{u}^n = \boldsymbol{P}_{\text{ext}} - {}^{t+\Delta t}\boldsymbol{F}_{Fint}^{(n-1)} \tag{114}$$

where $\ddot{\boldsymbol{U}}^n$ and $\dot{\boldsymbol{U}}^n$ are the realizations of the acceleration and speed vectors at time $t+\Delta t$ when iteration n is performed, and ${}^{t+\Delta t}\boldsymbol{u}^n$ is the displacement vector (not known yet) that is calculated at iteration n and referred to the previous iteration; that is, it is referred to the coordinates at the beginning of iteration n. Considering the definition of cumulative-displacement vector, it is clear that the cumulative-displacement vector at time $t+\Delta t$, when iteration n is completed, is the summation of the cumulative-displacement vector at time $t+\Delta t$ at iteration $(n-1)$ and the displacement vector (not known yet) of iteration n:

$${}^{t+\Delta t}\boldsymbol{U}^n = {}^{t+\Delta t}\boldsymbol{U}^{(n-1)} + {}^{t+\Delta t}\boldsymbol{u}^n \tag{115}$$

Using Eq. (115), the acceleration and velocity vectors become

$$\begin{aligned} &{}^{t+\Delta t}\boldsymbol{U}^n = {}^{t+\Delta t}\boldsymbol{U}_{\text{nd}}^n + {}^{t+\Delta t}\boldsymbol{u}^n \qquad {}^{t+\Delta t}\dot{\boldsymbol{U}}^n = {}^{t+\Delta t}\dot{\boldsymbol{U}}_{\text{nd}}^n + a_7 a_0{}^{t+\Delta t}\boldsymbol{u}^n \\ &{}^{t+\Delta t}\ddot{\boldsymbol{U}}^n = {}^{t+\Delta t}\ddot{\boldsymbol{U}}_{\text{nd}}^n + a_0{}^{t+\Delta t}\boldsymbol{u}^n \end{aligned} \tag{116}$$

where

$$\begin{aligned} &{}^{t+\Delta t}\boldsymbol{U}_{\text{nd}}^n = {}^{t+\Delta t}\boldsymbol{U}^{(n-1)} \\ &{}^{t+\Delta t}\dot{\boldsymbol{U}}_{\text{nd}}^n = {}^{t}\dot{\boldsymbol{U}} + a_6{}^{t}\ddot{\boldsymbol{U}} + a_7 a_0{}^{t+\Delta t}\boldsymbol{U}^{(n-1)} - a_7 a_0{}^{t}\boldsymbol{U} - a_7 a_2{}^{t}\dot{\boldsymbol{U}} \\ &\quad - a_7 a_3{}^{t}\ddot{\boldsymbol{U}} \\ &{}^{t+\Delta t}\ddot{\boldsymbol{U}}_{\text{nd}}^n = a_0{}^{t+\Delta t}\boldsymbol{U}^{(n-1)} - a_0{}^{t}\boldsymbol{U} - a_2{}^{t}\dot{\boldsymbol{U}} - a_3{}^{t}\ddot{\boldsymbol{U}} \end{aligned} \tag{117}$$

This compact form has the advantage that the terms that multiply the displacements of the current iterations are clearly separated. This is important in the definition of the tangent matrix of the entire system (the so-called effective tangent matrix). Substituting Eq. (116) into Eq. (114),

$$\begin{aligned} &\boldsymbol{M} \cdot [{}^{t+\Delta t}\ddot{\boldsymbol{U}}_{\text{nd}}^n + a_0{}^{t+\Delta t}\boldsymbol{u}^n] + \boldsymbol{C}_D \cdot [{}^{t+\Delta t}\dot{\boldsymbol{U}}_{\text{nd}}^n + a_7 a_0{}^{t+\Delta t}\boldsymbol{u}^n] \\ &\quad + {}^{t+\Delta t}\boldsymbol{K}_T^n \cdot {}^{t+\Delta t}\boldsymbol{u}^n = {}^{t+\Delta t}\boldsymbol{P}_{\text{ext}} - {}^{t+\Delta t}\boldsymbol{F}_{\text{int}}^{(n-1)} \end{aligned} \tag{118}$$

leading to

$$\begin{aligned} [{}^{t+\Delta t}\boldsymbol{K}_T^n + a_0\boldsymbol{M} + a_7 a_0 \boldsymbol{C}_D] \cdot {}^{t+\Delta t}\boldsymbol{u}^n &= {}^{t+\Delta t}\boldsymbol{P}_{\text{ext}} \\ -\boldsymbol{M} \cdot {}^{t+\Delta t}\ddot{\boldsymbol{U}}_{\text{nd}}^n - \boldsymbol{C}_D \cdot {}^{t+\Delta t}\dot{\boldsymbol{U}}_{\text{nd}}^n - {}^{t+\Delta t}\boldsymbol{F}_{\text{int}}^{(n-1)} \end{aligned} \tag{119}$$

or

$$[{}^{t+\Delta t}\boldsymbol{K}_T^n + \boldsymbol{K}_{T_{\text{dyn}}}^{\text{system}}] \cdot {}^{t+\Delta t}\boldsymbol{u}^n = {}^{t+\Delta t}\boldsymbol{P}_{\text{ext}} + {}^{t+\Delta t}\boldsymbol{P}_{\text{dyn}}^n - {}^{t+\Delta t}\boldsymbol{F}^{(n-1)} \tag{120}$$

or

$${}^{t+\Delta t}\boldsymbol{K}_{T\text{eff}}^n \cdot {}^{t+\Delta t}\boldsymbol{u}^n = {}^{t+\Delta t}\boldsymbol{P}_{\text{eff}}^n - {}^{t+\Delta t}\boldsymbol{F}^{(n-1)} \tag{121}$$

where ${}^{t+\Delta t}\boldsymbol{K}_{T\text{eff}}^n$ is the effective tangent matrix, $\boldsymbol{K}_{T_{\text{dyn}}}^{\text{system}}$ is the dynamic contribution (constant) to the effective tangent matrix, and ${}^{t+\Delta t}\boldsymbol{P}_{\text{eff}}^n$ are the effective loads, including the dynamic effects ${}^{t+\Delta t}\boldsymbol{P}_{\text{dyn}}^n$. We have

$$\begin{aligned} {}^{t+\Delta t}\boldsymbol{K}_{\text{eff}}^n &= {}^{t+\Delta t}\boldsymbol{K}_T^n + \boldsymbol{K}_{T_{\text{dyn}}}^{\text{system}} \\ \boldsymbol{K}_{T_{\text{dyn}}}^{\text{system}} &= a_0\boldsymbol{M} + a_7 a_0 \boldsymbol{C}_D \\ {}^{t+\Delta t}\boldsymbol{P}_{\text{eff}}^n &= {}^{t+\Delta t}\boldsymbol{P}_{\text{ext}} + {}^{t+\Delta t}\boldsymbol{P}_{\text{dyn}}^n \\ {}^{t+\Delta t}\boldsymbol{P}_{\text{dyn}}^n &= -\boldsymbol{M} \cdot {}^{t+\Delta t}\ddot{\boldsymbol{U}}_{\text{nd}}^n - \boldsymbol{C}_D \cdot {}^{t+\Delta t}\dot{\boldsymbol{U}}_{\text{nd}}^n \end{aligned} \tag{122}$$

The iterative procedure of a more general case with motion-dependent aerodynamic loads is explained next.

XIII. Newmark's Time-Integration Unsteady Newton–Raphson Method with Unsteady Aerodynamics

Suppose that there are both unsteady nonaerodynamic and aerodynamic loads. The equation that has to be solved at each iteration is [also see Eq. (114)]

$$\begin{aligned} &\boldsymbol{M} \cdot {}^{t+\Delta t}\ddot{\boldsymbol{U}}^n + \boldsymbol{C}_D \cdot {}^{t+\Delta t}\dot{\boldsymbol{U}}^n + {}^{t+\Delta t}\boldsymbol{K}_T^n \cdot {}^{t+\Delta t}\boldsymbol{u}^n \\ &\quad = {}^{t+\Delta t}\boldsymbol{P}_{\text{ext}} + {}^{t+\Delta t}\boldsymbol{L}_{\text{unsteady}}^n - {}^{t+\Delta t}\boldsymbol{F}_{\text{int}}^{(n-1)} \end{aligned} \tag{123}$$

where ${}^{t+\Delta t}\boldsymbol{L}_{\text{unsteady}}^n$ is the nth realization of the aerodynamic loads at time $t+\Delta t$. The explicit form of the loads is [see Eq. (103)]

$$ {}^{t+\Delta t}\boldsymbol{L}^{n}_{\text{unsteady}} = \boldsymbol{\mathcal{A}}^{\star} \cdot {}^{t+\Delta t}\boldsymbol{U}^{n} + \boldsymbol{\mathcal{A}}^{\star}_{1} \cdot {}^{t+\Delta t}\dot{\boldsymbol{U}}^{n} + \boldsymbol{\mathcal{A}}^{\star}_{2} \cdot {}^{t+\Delta t}\ddot{\boldsymbol{U}}^{n} - \sum_{i=1}^{N_{\text{lag}}} \bar{\beta}_i \boldsymbol{\mathcal{A}}^{\star}_{2+i} \int_0^{t+\Delta t} {}^{\tau}\boldsymbol{U}^{n} e^{-\bar{\beta}_i (t+\Delta t-\tau)}\, \mathrm{d}\tau \tag{124} $$

A short discussion is in order regarding the time step. Considering that Newmark's method for time integration is implicit, the time step can be relatively large. However, the aerodynamic-force models are based on forces obtained in the frequency domain by using set of modes and tabulated reduced frequencies. The maximum reduced frequency used for the aerodynamic simulation in the frequency domain and at which we can expect the Roger approximation to still be accurate is

$$ k^{\star}_{\max} = \frac{\omega_{\max} b}{V_{\infty}} \tag{125} $$

The maximum circular frequency, for which the generalized aerodynamics model has meaning, is then

$$ \omega_{\max} = \frac{k^{\star}_{\max} V_{\infty}}{b} \tag{126} $$

The associated frequency is

$$ f_{\max} = \frac{\omega_{\max}}{2\pi} = \frac{k^{\star}_{\max} V_{\infty}}{2\pi b} \tag{127} $$

The associated period is therefore

$$ T_{\min} = \frac{1}{f_{\max}} = \frac{2\pi b}{k^{\star}_{\max} V_{\infty}} \tag{128} $$

To have a meaningful representation of the unsteady aerodynamic forces, the time-step size should be smaller than $T_{\min}$ to allow capturing (in the time simulation) the highest frequency for which the model is valid. For example, we could take

$$ \Delta t = \frac{T_{\min}}{N_{\text{time step}}} \tag{129} $$

where $N_{\text{time step}} \geq 1$ is chosen by the user. We focus now on the generic time step over the interval $t \leq \tau \leq t + \Delta t$.

To express the aerodynamic forces, we need to calculate the integrals on the RHS of Eq. (124). In the formulation so far, the integrals already involve the equilibrium solution at time $t + \Delta t$ and this solution is not known. Moreover, the change over time of the cumulative-displacement vector is also not known. To overcome these issues, consider the generic integral ${}^{t+\Delta t}\boldsymbol{I}_i$ of the lag term i:

$$ {}^{t+\Delta t}\boldsymbol{I}_i \doteq \int_0^{t+\Delta t} {}^{\tau}\boldsymbol{U} e^{-\bar{\beta}_i (t+\Delta t-\tau)}\, \mathrm{d}\tau \tag{130} $$

Because the time-step size is smaller than the minimum period of the considered aerodynamic forces [see Eq. (129)], it is reasonable to assume that the cumulative displacement at time $t + \Delta t$ (actually, its approximation given by the nth iteration) and the cumulative displacement at a time τ (with the obvious condition $t \leq \tau \leq t + \Delta t$ in the interval) are related by a linear relation. The following relation can now be written (${}^{\tau}\boldsymbol{U}^{n}$ is the nth realization of the quantity ${}^{\tau}\boldsymbol{U}$):

$$ \frac{{}^{t+\Delta t}\boldsymbol{U}^{n} - {}^{t}\boldsymbol{U}}{t + \Delta t - t} = \frac{{}^{\tau}\boldsymbol{U}^{n} - {}^{t}\boldsymbol{U}}{\tau - t} \qquad t \leq \tau \leq t + \Delta t \tag{131} $$

Using the definition

$$ {}^{t+\Delta t}\boldsymbol{U}^{\star n}_{\text{nd}} \doteq {}^{t+\Delta t}\boldsymbol{U}^{n}_{\text{nd}} - {}^{t}\boldsymbol{U} = {}^{t+\Delta t}\boldsymbol{U}^{(n-1)} - {}^{t}\boldsymbol{U} $$

we finally obtain

$$ {}^{\tau}\boldsymbol{U}^{n} = \left[\frac{{}^{t+\Delta t}\boldsymbol{u}^{n}}{\Delta t} + \frac{{}^{t+\Delta t}\boldsymbol{U}^{\star n}_{\text{nd}}}{\Delta t} \right] \tau + \left[-\frac{{}^{t+\Delta t}\boldsymbol{u}^{n}}{\Delta t} t - \frac{{}^{t+\Delta t}\boldsymbol{U}^{\star n}_{\text{nd}}}{\Delta t} t + {}^{t}\boldsymbol{U} \right] \tag{132} $$

Based on Eq. (130), the following identity holds:

$$ {}^{t+\Delta t}\boldsymbol{I}_i = e^{-\bar{\beta}_i \Delta t} \cdot {}^{t}\boldsymbol{I}_i + e^{-\bar{\beta}_i (t+\Delta t)} \int_t^{t+\Delta t} {}^{\tau}\boldsymbol{U} e^{\bar{\beta}_i \tau}\, \mathrm{d}\tau \tag{133} $$

The nth realization of the integral ${}^{t+\Delta t}\boldsymbol{I}_i$ of the generic lag term is [see Eq. (133)]

$$ {}^{t+\Delta t}\boldsymbol{I}^{n}_i = e^{-\bar{\beta}_i \Delta t} \cdot {}^{t}\boldsymbol{I}_i + e^{-\bar{\beta}_i (t+\Delta t)} \int_t^{t+\Delta t} {}^{\tau}\boldsymbol{U}^{n} e^{\bar{\beta}_i \tau}\, \mathrm{d}\tau \tag{134} $$

Equation (134) can be further developed if the cumulative-displacement vector is approximated using Eq. (132) and leads to simple integrals that can be obtained analytically. To calculate the integral on the RHS for the function ${}^{\tau}\boldsymbol{U}$, we use its approximation in the integration domain [see Eq. (132)]. After some algebra, the following formula is reached:

$$ {}^{t+\Delta t}\boldsymbol{I}^{n}_i = {}^{t+\Delta t}\boldsymbol{I}^{\star n}_i + \frac{{}^{t+\Delta t}\boldsymbol{u}^{n}}{\Delta t} \Lambda_i \tag{135} $$

where

$$ {}^{t+\Delta t}\boldsymbol{I}^{\star n}_i = e^{-\bar{\beta}_i \Delta t} \cdot {}^{t}\boldsymbol{I}_i + \frac{{}^{t+\Delta t}\boldsymbol{U}^{\star n}_{\text{nd}}}{\Delta t} \Lambda_i + {}^{t}\boldsymbol{U} \lambda_i \qquad \Lambda_i = \frac{e^{-\bar{\beta}_i \Delta t} + \bar{\beta}_i \Delta t - 1}{\bar{\beta}_i^2} \qquad \lambda_i = \frac{1 - e^{-\bar{\beta}_i \Delta t}}{\bar{\beta}_i} \tag{136} $$

All the terms needed to evaluate the unsteady aerodynamic-force vector expressed in Eq. (124) are now available. Using Eq. (116), the aerodynamic-force vector is written as

$$ {}^{t+\Delta t}\boldsymbol{L}^{n}_{\text{unsteady}} = \boldsymbol{\mathcal{A}}^{\star} \cdot {}^{t+\Delta t}\boldsymbol{U}^{n}_{\text{nd}} + \boldsymbol{\mathcal{A}}^{\star}_{1} \cdot {}^{t+\Delta t}\dot{\boldsymbol{U}}^{n}_{\text{nd}} + \boldsymbol{\mathcal{A}}^{\star}_{2} \cdot {}^{t+\Delta t}\ddot{\boldsymbol{U}}^{n}_{\text{nd}} - \sum_{i=1}^{N_{\text{lag}}} \bar{\beta}_i \boldsymbol{\mathcal{A}}^{\star}_{2+i} {}^{t+\Delta t}\boldsymbol{I}^{\star n}_i + \Big[\boldsymbol{\mathcal{A}}^{\star} + a_7 a_0 \boldsymbol{\mathcal{A}}^{\star}_{1} + a_0 \boldsymbol{\mathcal{A}}^{\star}_{2} - \sum_{i=1}^{N_{\text{lag}}} \frac{\bar{\beta}_i \Lambda_i}{\Delta t} \boldsymbol{\mathcal{A}}^{\star}_{2+i} \Big] {}^{t+\Delta t}\boldsymbol{u}^{n} \tag{137} $$

The final system of equations that has to be solved is similar to that obtained for the pure mechanical case with no aerodynamics. We have

$$ {}^{t+\Delta t}\boldsymbol{K}^{n}_{T\text{eff}} \cdot {}^{t+\Delta t}\boldsymbol{u}^{n} = {}^{t+\Delta t}\boldsymbol{P}^{n}_{\text{eff}} - {}^{t+\Delta t}\boldsymbol{F}^{(n-1)} \tag{138} $$

where

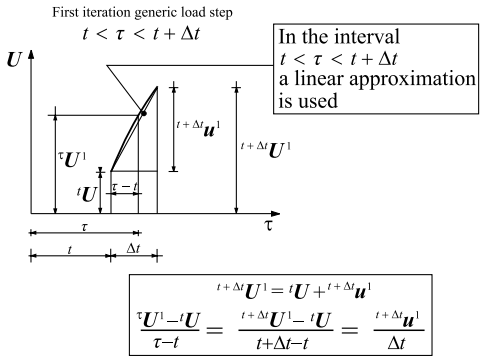

Fig. 4 Approximation used for the calculations of the integrals containing the lag terms (first iteration of the generic load step).

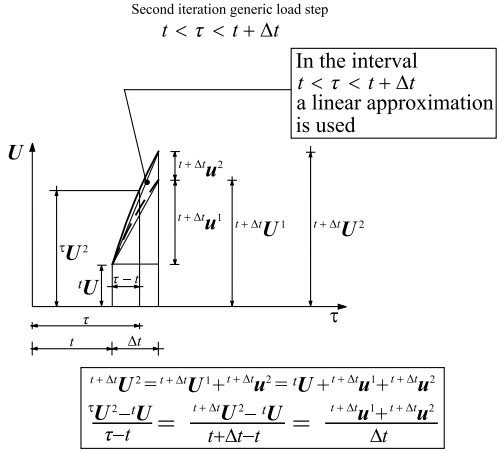

Fig. 5 Approximation used for the calculations of the integrals containing the lag terms (second iteration of the generic load step).

$$
\begin{aligned}
&{}^{t+\Delta t}\boldsymbol{K}^n_{T\text{eff}} = {}^{t+\Delta t}\boldsymbol{K}^n_T + \boldsymbol{K}^{\text{system}}_{T_{\text{dyn}}} + \boldsymbol{K}^{\text{system}}_{T_{\text{aero}}}\\
&\boldsymbol{K}^{\text{system}}_{T_{\text{aero}}} = a_0\boldsymbol{M} + a_7 a_0 \boldsymbol{C}_D\\
&\boldsymbol{K}^{\text{system}}_{T_{\text{aero}}} = -\boldsymbol{\mathcal{A}}^{\star} - a_7 a_0 \boldsymbol{\mathcal{A}}^{\star}_1 - a_0 \boldsymbol{\mathcal{A}}^{\star}_2 + \sum_{i=1}^{N_{\text{lag}}} \frac{\bar{\beta}_i \Lambda_i}{\Delta t} \boldsymbol{\mathcal{A}}^{\star}_{2+i}\\
&{}^{t+\Delta t}\boldsymbol{P}^n_{\text{eff}} = {}^{t+\Delta t}\boldsymbol{P}_{\text{ext}} + {}^{t+\Delta t}\boldsymbol{P}^n_{\text{dyn}} + {}^{t+\Delta t}\boldsymbol{P}^n_{\text{aero}}\\
&{}^{t+\Delta t}\boldsymbol{P}^n_{\text{dyn}} = -\boldsymbol{M} \cdot {}^{t+\Delta t}\ddot{\boldsymbol{U}}^n_{\text{nd}} - \boldsymbol{C}_D \cdot {}^{t+\Delta t}\dot{\boldsymbol{U}}^n_{\text{nd}}\\
&{}^{t+\Delta t}\boldsymbol{P}^n_{\text{aero}} = \boldsymbol{\mathcal{A}}^{\star} \cdot {}^{t+\Delta t}\boldsymbol{U}^n_{\text{nd}} + \boldsymbol{\mathcal{A}}^{\star}_1 \cdot {}^{t+\Delta t}\dot{\boldsymbol{U}}^n_{\text{nd}} + \boldsymbol{\mathcal{A}}^{\star}_2 \cdot {}^{t+\Delta t}\ddot{\boldsymbol{U}}^n_{\text{nd}}\\
&\quad - \sum_{i=1}^{N_{\text{lag}}} \bar{\beta}_i \boldsymbol{\mathcal{A}}^{\star}_{2+i} {}^{t+\Delta t}\boldsymbol{I}^{\star n}_i
\end{aligned}
\tag{139}
$$

Figures 4 and 5 show how the displacements are approximated in time to calculate the lag term integrals. Note that the approximation is more accurate if the size of the step used in the time integration is small. It may be argued that if the time step is too small, aerodynamics for reduced frequencies beyond the maximum reduced frequency used in the calculation of the aerodynamic generalized matrices are included. This is true in theory, but numerical experiments shown in this paper demonstrate the convergence when the time step is reduced. Filtering of any errors due to high-frequency behavior is also due to the stability of the Newmark method.

$\boldsymbol{C}_D$ is the full-order damping matrix. In this paper, a viscous damping model is used as follows: the reference generalized damping matrix is built considering a set of modes that are, in general, not coincident with the basis used to define the aerodynamic generalized matrices. Then the reference generalized damping matrix is expanded to be of the same order as the generalized aerodynamic matrices. This operation is done by considering (as a new set of modes) the same modes used to define the generalized aerodynamic matrices and the transformation matrix $\boldsymbol{T}$ and by applying the least-squares method to move from one set of modes to another. The generalized damping matrix is obtained in the same modal coordinates as the generalized aerodynamic matrix. Finally, the full-order damping matrix $\boldsymbol{C}_D$ is obtained from the generalized damping matrix by using a transformation similar to Eq. (90).

XIV. Newmark's Method and Unsteady Aerodynamics: Iterative Procedure

The preceding procedures can now be summarized.

A. Initial Calculations

For the initial calculations, the maximum size step is chosen by using

$$
\Delta t = \frac{T_{\min}}{N_{\text{time step}}} = \frac{2\pi b}{k^{\star}_{\max} V_{\infty} N_{\text{time step}}} \tag{140}
$$

where $k^{\star}_{\max} = \omega_{\max} b / V_{\infty}$ is the maximum reduced frequency used for the Roger fit, and $N_{\text{time step}}$ is a number chosen by the user. If this number is larger, the lag terms are more accurately calculated. CPU time increases considerably, however, when $N_{\text{time step}}$ is large. Next, the following quantities are calculated:

$$
\begin{aligned}
&a_0 = \frac{1}{\alpha(\Delta t)^2} \qquad a_1 = \frac{\delta}{\alpha \Delta t} \qquad a_2 = \frac{1}{\alpha \Delta t} \qquad a_3 = \frac{1}{2\alpha} - 1\\
&a_4 = \frac{\delta}{\alpha} - 1 \qquad a_5 = \frac{\Delta t}{2}\left(\frac{\delta}{\alpha} - 2\right) \qquad a_6 = \Delta t(1 - \delta)\\
&a_7 = \delta \Delta t
\end{aligned}
\tag{141}
$$

where $\delta = \frac{1}{2}$ and $\alpha = \frac{1}{4}$.

The parameters used in the derivation of the aerodynamic contribution are

$$
\bar{\beta}_i = \frac{V_{\infty}}{b}\beta_i \qquad \Lambda_i = \frac{e^{-\bar{\beta}_i \Delta t} + \bar{\beta}_i \Delta t - 1}{\bar{\beta}_i^2} \qquad \lambda_i = \frac{1 - e^{-\bar{\beta}_i \Delta t}}{\bar{\beta}_i} \tag{142}
$$

For calculation of the dynamic contribution $\boldsymbol{K}^{\text{system}}_{T_{\text{dyn}}}$ to the effective tangent matrix (in the present formulation, this contribution is constant), we have

$$
\boldsymbol{K}^{\text{system}}_{T_{\text{dyn}}} = +a_0\boldsymbol{M} + a_7 a_0 \boldsymbol{C}_D \tag{143}
$$

The contribution to the tangent matrix due to the aerodynamic part is

$$
\boldsymbol{K}^{\text{system}}_{T_{\text{aero}}} = -\boldsymbol{\mathcal{A}}^{\star} - a_7 a_0 \boldsymbol{\mathcal{A}}^{\star}_1 - a_0 \boldsymbol{\mathcal{A}}^{\star}_2 + \sum_{i=1}^{N_{\text{lag}}} \frac{\bar{\beta}_i \Lambda_i}{\Delta t} \boldsymbol{\mathcal{A}}^{\star}_{2+i} \tag{144}
$$

This contribution does not depend on the load step or iteration and it is calculated once.

B. Time-Step Calculations

For the time-step calculations of the external loads ${}^{t+\Delta t}\boldsymbol{P}_{\text{ext}}$ using the assigned temporal law, note that each time step defines a variation of the parameters over the interval $[t, t + \Delta t]$. Some auxiliary quantities are calculated:

$$
\begin{aligned}
&{}^{t+\Delta t}\boldsymbol{U}^n_{\text{nd}} = {}^{t+\Delta t}\boldsymbol{U}^{(n-1)}\\
&{}^{t+\Delta t}\dot{\boldsymbol{U}}^n_{\text{nd}} = {}^{t}\dot{\boldsymbol{U}} + a_6 {}^{t}\ddot{\boldsymbol{U}} + a_7 a_0 {}^{t+\Delta t}\boldsymbol{U}^{(n-1)} - a_7 a_0 {}^{t}\boldsymbol{U} - a_7 a_2 {}^{t}\dot{\boldsymbol{U}}\\
&\quad - a_7 a_3 {}^{t}\ddot{\boldsymbol{U}}\\
&{}^{t+\Delta t}\ddot{\boldsymbol{U}}^n_{\text{nd}} = a_0 {}^{t+\Delta t}\boldsymbol{U}^{(n-1)} - a_0 {}^{t}\boldsymbol{U} - a_2 {}^{t}\dot{\boldsymbol{U}} - a_3 {}^{t}\ddot{\boldsymbol{U}}\\
&{}^{t+\Delta t}\boldsymbol{U}^{\star n}_{\text{nd}} = {}^{t+\Delta t}\boldsymbol{U}^n_{\text{nd}} - {}^{t}\boldsymbol{U} = {}^{t+\Delta t}\boldsymbol{U}^{(n-1)} - {}^{t}\boldsymbol{U}\\
&{}^{t+\Delta t}\boldsymbol{I}^{\star n}_i = e^{-\bar{\beta}_i \Delta t} \cdot {}^{t}\boldsymbol{I}_i + \frac{{}^{t+\Delta t}\boldsymbol{U}^{\star n}_{\text{nd}}}{\Delta t}\Lambda_i + \boldsymbol{U}\lambda_i
\end{aligned}
\tag{145}
$$

This operation is performed at each iteration. If the first iteration of the current load step is considered, then the previous realization of the cumulative displacement will be ${}^{t+\Delta t}\boldsymbol{U}^{(n-1)} = {}^{t}\boldsymbol{U}$. If the very first iteration is considered, then all the quantities are coincident with the initial (if different from zero) values. For example, ${}^{t}\boldsymbol{U} = {}^{0}\boldsymbol{U}$; in this particular case, it is also ${}^{t}\boldsymbol{I}_i = {}^{0}\boldsymbol{I}_i = \boldsymbol{0}$, because the integrals are performed over an interval that is zero.

The loads are also calculated:

$$
\begin{aligned}
{}^{t+\Delta t}\boldsymbol{P}^n_{\text{dyn}} &= -\boldsymbol{M}\cdot {}^{t+\Delta t}\ddot{\boldsymbol{U}}^n_{\text{nd}} - \boldsymbol{C}_D\cdot {}^{t+\Delta t}\dot{\boldsymbol{U}}^n_{\text{nd}}\\
{}^{t+\Delta t}\boldsymbol{P}^n_{\text{aero}} &= \boldsymbol{\mathcal{A}}^\star\cdot {}^{t+\Delta t}\boldsymbol{U}^n_{\text{nd}} + \boldsymbol{\mathcal{A}}^\star_1\cdot {}^{t+\Delta t}\dot{\boldsymbol{U}}^n_{\text{nd}} + \boldsymbol{\mathcal{A}}^\star_2\cdot {}^{t+\Delta t}\ddot{\boldsymbol{U}}^n_{\text{nd}}\\
&\quad - \sum_{i=1}^{N_{\text{lag}}} \bar{\beta}_i \boldsymbol{\mathcal{A}}^\star_{2+i}\, {}^{t+\Delta t}\boldsymbol{I}^{\star n}_i\\
{}^{t+\Delta t}\boldsymbol{P}^n_{\text{eff}} &= {}^{t+\Delta t}\boldsymbol{P}_{\text{ext}} + {}^{t+\Delta t}\boldsymbol{P}^n_{\text{dyn}} + {}^{t+\Delta t}\boldsymbol{P}^n_{\text{aero}}
\end{aligned}
\tag{146}
$$

The external loads ${}^{t+\Delta t}\boldsymbol{P}_{\text{ext}}$ change only when another time step is considered. Regarding the calculation of the effective tangent matrix,

$$
{}^{t+\Delta t}\boldsymbol{K}^n_{T\text{eff}} = {}^{t+\Delta t}\boldsymbol{K}^n_T + \boldsymbol{K}^{\text{system}}_{T_{\text{dyn}}} + \boldsymbol{K}^{\text{system}}_{T_{\text{aero}}} \tag{147}
$$

The linear system is solved:

$$
{}^{t+\Delta t}\boldsymbol{K}^n_{T_{\text{eff}}}\cdot {}^{t+\Delta t}\boldsymbol{u}^n = {}^{t+\Delta t}\boldsymbol{P}^n_{\text{eff}} - {}^{t+\Delta t}\boldsymbol{F}^{(n-1)}_{\text{int}} \tag{148}
$$

The displacements ${}^{t+\Delta t}\boldsymbol{u}^n$ are used to update the coordinates of the nodes.

The cumulative-displacement vector is updated for the next iteration:

$$
{}^{t+\Delta t}\boldsymbol{U}^n = {}^{t+\Delta t}\boldsymbol{U}^{(n-1)} + {}^{t+\Delta t}\boldsymbol{u}^n \tag{149}
$$

The internal forces ${}^{t+\Delta t}\boldsymbol{F}^n_{\text{int}}$ are calculated for the next iteration. Another iteration is performed unless the convergence criteria is satisfied. If so, the iterative process in the time step is considered complete and the vectors are updated.

$$
\begin{aligned}
{}^{t+\Delta t}\boldsymbol{U} &= {}^{t+\Delta t}\boldsymbol{U}^n = {}^{t+\Delta t}\boldsymbol{U}^n_{\text{nd}} + {}^{t+\Delta t}\boldsymbol{u}^n\\
{}^{t+\Delta t}\dot{\boldsymbol{U}} &= {}^{t+\Delta t}\dot{\boldsymbol{U}}^n = {}^{t+\Delta t}\dot{\boldsymbol{U}}^n_{\text{nd}} + a_7 a_0\, {}^{t+\Delta t}\boldsymbol{u}^n\\
{}^{t+\Delta t}\ddot{\boldsymbol{U}} &= {}^{t+\Delta t}\ddot{\boldsymbol{U}}^n = {}^{t+\Delta t}\ddot{\boldsymbol{U}}^n_{\text{nd}} + a_0\, {}^{t+\Delta t}\boldsymbol{u}^n\\
{}^{t+\Delta t}\boldsymbol{I}_i &= {}^{t+\Delta t}\boldsymbol{I}^n_i = e^{-\bar{\beta}_i\Delta t}\cdot {}^{t}\boldsymbol{I}_i + \frac{{}^{t+\Delta t}\boldsymbol{U} - {}^{t}\boldsymbol{U}}{\Delta t}\Lambda_i + {}^{t}\boldsymbol{U}\lambda_i
\end{aligned}
\tag{150}
$$

The process restarts with the updating of the time: $t \to t + \Delta t$.

The updating of the integrals involving the lag terms in Eq. (150) is derived as follows:

$$
\begin{aligned}
{}^{t+\Delta t}\boldsymbol{I}_i &= {}^{t+\Delta t}\boldsymbol{I}^n_i = {}^{t+\Delta t}\boldsymbol{I}^{\star n}_i + \frac{{}^{t+\Delta t}\boldsymbol{u}^n}{\Delta t}\Lambda_i = e^{-\bar{\beta}_i\Delta t}\cdot {}^{t}\boldsymbol{I}_i\\
&\quad + \frac{{}^{t+\Delta t}\boldsymbol{U}^{\star n}_{\text{nd}}}{\Delta t}\Lambda_i + \frac{{}^{t+\Delta t}\boldsymbol{u}^n}{\Delta t}\Lambda_i + {}^{t}\boldsymbol{U}\lambda_i = e^{-\bar{\beta}_i\Delta t}\cdot {}^{t}\boldsymbol{I}_i\\
&\quad + \frac{{}^{t+\Delta t}\boldsymbol{U}^n - {}^{t}\boldsymbol{U}}{\Delta t}\Lambda_i + {}^{t}\boldsymbol{U}\lambda_i = e^{-\bar{\beta}_i\Delta t}\cdot {}^{t}\boldsymbol{I}_i + \frac{{}^{t+\Delta t}\boldsymbol{U} - {}^{t}\boldsymbol{U}}{\Delta t}\Lambda_i\\
&\quad + {}^{t}\boldsymbol{U}\lambda_i
\end{aligned}
\tag{151}
$$

C. Initial Conditions

The unsteady aerodynamic forces in the time domain are given in Eq. (103). If this formula is written for the initial instant $t = 0$, the integral of the lag terms is zero because the limits of the integral are coincident, and so we have

$$
{}^{0}\boldsymbol{L}_{\text{unsteady}} = \boldsymbol{\mathcal{A}}^\star\cdot {}^{0}\boldsymbol{U} + \boldsymbol{\mathcal{A}}^\star_1\cdot {}^{0}\dot{\boldsymbol{U}} + \boldsymbol{\mathcal{A}}^\star_2\cdot {}^{0}\ddot{\boldsymbol{U}} \tag{152}
$$

It is reasonable to assume that the speed of nodal motion (not the aerodynamic speed V_∞, which is different from zero) is zero:

$$
{}^{0}\dot{\boldsymbol{U}} = 0 \tag{153}
$$

The aerodynamic-force vector is then

$$
{}^{0}\boldsymbol{L}_{\text{unsteady}} = \boldsymbol{\mathcal{A}}^\star\cdot {}^{0}\boldsymbol{U} + \boldsymbol{\mathcal{A}}^\star_2\cdot {}^{0}\ddot{\boldsymbol{U}} \tag{154}
$$

The lag terms are still present in the aerodynamic stiffness matrix $\boldsymbol{\mathcal{A}}^\star$. We next assume a perturbed initial configuration $\boldsymbol{x}^{\text{pert}}$ (for example, a configuration with a small angle of attack), and so it is important that

$$
\boldsymbol{x}^{\text{pert}} \neq \boldsymbol{x}^{\alpha=0} \tag{155}
$$

Based on this assumption, we augment the vectors $\boldsymbol{x}^{\text{pert}}$ and $\boldsymbol{x}^{\alpha=0}$ by adding zeros in correspondence of the rotation degrees of freedom of the structural nodes, and we get the vectors $\bar{\boldsymbol{x}}^{\text{pert}}$ and $\bar{\boldsymbol{x}}^{\alpha=0}$, respectively. The cumulative displacement at the initial instant is according to the following formula:

$$
{}^{0}\boldsymbol{U} = \bar{\boldsymbol{x}}^{\text{pert}} - \bar{\boldsymbol{x}}^{\alpha=0} \tag{156}
$$

The aerodynamic loads are then partially known, and to find the acceleration, we consider the equilibrium equation written at the initial instant $t = 0$ and we consider that the nodal speeds are zero. We then have [see Eq. (123)]

$$
\boldsymbol{M}\cdot {}^{0}\ddot{\boldsymbol{U}} = {}^{0}\boldsymbol{P}_{\text{ext}} + {}^{0}\boldsymbol{L}_{\text{unsteady}} - {}^{0}\boldsymbol{F}_{\text{int}} \tag{157}
$$

Suppose now that the initial condition is stress-free. No internal

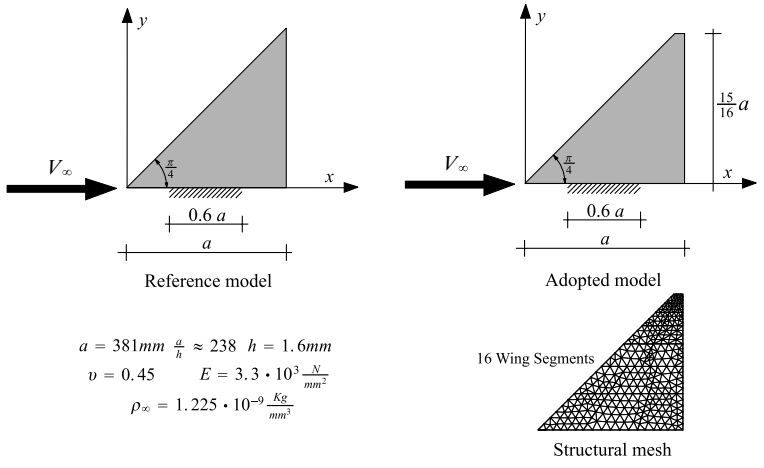

Fig. 6 Test model 1: delta wing.

forces are present therefore, and with the help of Eq. (154), we can write

$$\boldsymbol{M} \cdot {}^0\ddot{\boldsymbol{U}} = {}^0\boldsymbol{P}_{\text{ext}} + \boldsymbol{\mathcal{A}}^{\star} \cdot {}^0\boldsymbol{U} + \boldsymbol{\mathcal{A}}_2^{\star} \cdot {}^0\ddot{\boldsymbol{U}} \tag{158}$$

from which we can get the initial value for the acceleration:

$${}^0\ddot{\boldsymbol{U}} = [\boldsymbol{M} - \boldsymbol{\mathcal{A}}_2^{\star}]^{-1} \cdot [{}^0\boldsymbol{P}_{\text{ext}} + \boldsymbol{\mathcal{A}}^{\star} \cdot {}^0\boldsymbol{U}] \tag{159}$$

With this formulation, even in the case of absence of nonaerodynamic loads (${}^0\boldsymbol{P}_{\text{ext}} = 0$), we have nonzero accelerations. The time-step procedure (Newmark and Newton–Raphson) can now be started with the initial conditions (153), (156), and (159) and with the initial coordinate vector $\boldsymbol{x}^{\text{pert}}$.

XV. Results

We consider steady and unsteady solutions using the proposed procedure. It must be pointed out that the steady part has been deeply revised and modified with respect to that presented in an earlier work by the authors [44]. Therefore, new steady numerical evaluations are reported here. As far as the steady simulation is concerned, the main difference between the former and the new approach is that now only a single aerodynamic matrix is used, whereas [44] three different matrices were used in an early work. The two approaches are exactly equivalent in the full-order case, in which aerodynamic matrices of the order of the number of all aerodynamic boxes in the aerodynamic model are used. But the formulations are not equivalent when the aerodynamic matrix $\boldsymbol{C}$ defined earlier is approximated with the procedure described in this paper. Two tests cases are selected for validation and evaluation of the new approach.

A. Test Model 1 Planar Case: Delta Wing

Test model 1 is a delta wing [23,24] for which both numerical and experimental results are available. Data for the mathematical model are as follows: 16 wing segments; 318 structural nodes, 552 structural (triangular) elements, 252 aerodynamic panels, 17 terms for Ueda's formulas used to generate the unsteady-kernel-function approximation for the doublet-lattice method, and $M = 0$.

Reduced frequencies (defined as $k^{\star} = \omega b / V_{\infty}$, where b is the half-root chord) used to generate a Roger model are 0, 0.02, 0.05, 0.1, 0.2, 0.3, 0.4, 0.5, 0.6, 0.7, 0.75, 0.8, 0.85, 0.9, 0.95, 1, 1.2, 1.4, 1.6, 1.8, and 2. The selected lag terms are $\beta_1 = 0.25$, $\beta_2 = 0.5$, $\beta_3 = 0.9$, $\beta_4 = 1.5$,$\beta_5 = 1.7$, and $\beta_6 = 2.0$. The geometry of the wing is shown in Fig. 6.

B. Test Model 2 Nonplanar Case: A Joined-Wing Configuration

For the second test case, a new configuration is created by adding a rear wing and attachment structure to the delta wing (see Fig. 7) to create a joined wing. No practical implementation of such a configuration is implied here. It is designed for studying the resulting aeroelastic behavior of a wing already known to be structurally nonlinear.

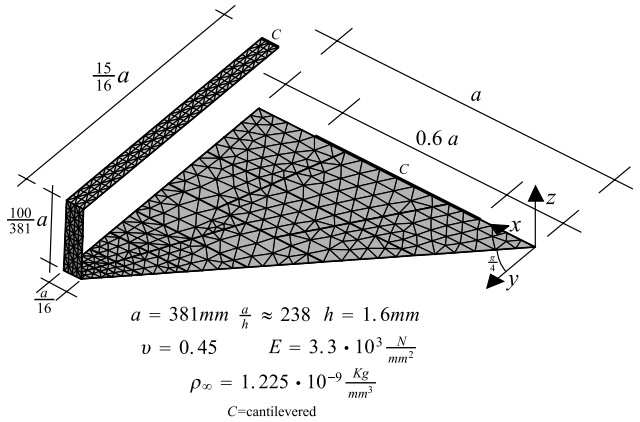

Fig. 7 Test model 2: joined-wing model derived from the delta wing.

Table 1 Delta-wing linear flutter speed and frequency comparison against MD Nastran

	Flutter speed, m/s	Flutter frequency, Hz
Present ($\zeta_i = 0$)	21.77	15.21
Present ($\zeta_i = 0.01$)	22.70	14.67
Present MD Nastran ($\zeta_i = 0$)	21.76	15.32

Data for the mathematical model (the joined wing) are as follows: 18 wing segments; 518 structural nodes, 872 structural (triangular) elements, 696 aerodynamic panels, 25 terms for Ueda's formulas used to generate the unsteady-kernel-function approximation for the doublet-lattice method, and $M = 0$.

Reduced frequencies used to generate a Roger model and lag terms are those used for the delta wing (test model 1).

C. Test Model 1 Linear Flutter Results: Comparison Against MD Nastran

The comparison shows excellent correlation (see Table 1). The p-k method was used in MD Nastran, whereas in the present capability the flutter speed, is calculated by using the root locus procedure based on a linear time-invariant state-space model. Twenty modes were used to calculate the generalized matrices. Viscous damping ratios are indicated with ζ_i, and the number of modes used to define reference generalized damping matrix is 20.

D. Test Model 1 Nonlinear Static Deflection with Full-Order Aerodynamic Matrices

Both the doublet-lattice method and the vortex-lattice method have yielded the same numerical results, demonstrating the good steady performances of the present doublet-lattice formulation. This is accordance with the literature [13,37], in which the correlation between DLM and VLM is very good with a similar approach. The correlation against nonlinear steady results[§] is very good. In particular, for a speed of 21 m/s and $\alpha = 1$ deg $= \pi/180$, the reference value[§] for the nondimensional tip displacement u_z/h is 8.80, whereas the present capability gives $u_z/h = 8.07$.

E. Test Model 1 Steady Case: Full-Order Structure and Reduced-Order Aerodynamics

Four different methods are used:

1) In method 1, the basis $\boldsymbol{\Psi}$ [see Eq. (72)] is built by using natural modes. However, the lumped mass matrix used to calculate the modes is modified by reducing the terms related to the u_x and u_y DOF by 99%. With this reduction, the modes mainly have the out-of-plane components, and the basis is more tailored to approximate the out-of-plane displacement u_z. The least-squares method is performed only on the component u_z. For general 3-D configurations, the out-of-plane component is not generally u_z.

2) In method 2, the basis $\boldsymbol{\Psi}$ is built by using natural modes. The mass matrix is not modified. The LSM is performed only on component u_z.

3) In method 3, the basis $\boldsymbol{\Psi}$ is built by using natural modes and the mass matrix is modified as in method 1. The LSM is performed on all the translational displacements u_x, u_y, and u_z.

4) In method 4, the basis $\boldsymbol{\Psi}$ is built by using natural modes and the mass matrix is not modified, as in method 2. The LSM is performed on all the translational displacements u_x, u_y, and u_z. This is the method used for most general 3-D configurations.

The effect of the different methods is reported in Table 2. It is clear that no significant difference is found when the different methods are used.

To model cases in which the wing is placed initially at a rigid angle of attack or with some initial shape, the modal basis $\boldsymbol{\Psi}$ is modified by replacing the last mode (last column in the matrix) by the initial

[§]Private communication with P. J. Attar, 13 March 2005.

Table 2 Delta-wing tip displacement u_z in millimeters. Full-order and approximated (10 modes) cases. Comparison between the different methods used in the construction of the approximated aerodynamic matrix. The DLM was used. The last mode is replaced by the quantity $\bar{x}^{\text{pert}} - \bar{x}^{\alpha=0}$. The excessive number of digits is used for clarity.

λ	V, m/s	Full order	Method 1	Method 2	Method 3	Method 4
5	8.57	2.7228	2.7218	2.7218	2.7218	2.7220
10	12.12	5.2197	5.2190	5.2190	5.2190	5.2195
15	14.85	7.4768	7.4770	7.4770	7.4770	7.4777
20	17.15	9.4994	9.5007	9.5007	9.5008	9.5015
25	19.17	11.3045	11.3071	11.3071	11.3071	11.3079
30	21.00	12.9147	12.9182	12.9182	12.9182	12.9190

shape. That is, the last mode is replaced by the difference $\bar{x}^{\text{pert}} - \bar{x}^{\alpha=0}$. The reference shape (the shape with no angle of attack of aerodynamic boxes) has to be subtracted because the modal base has to represent motion that is a perturbation with respect to the reference shape. The cases presented here for the delta wing involve the condition of a rigid angle of attack equal to 1 deg. The VLM (modified to be consistent with the DLM, and so the reference configuration has no angle of attack on aerodynamic boxes) and DLM do not show numerical differences. In all cases, the results are practically coincident.

If the last mode of the basis used to build the transformation matrix (adopted to convert the reduced-order aeromatrix to the full-order matrix) is replaced by the quantity $\bar{x}^{\text{pert}} - \bar{x}^{\alpha=0}$, the improvement is significant. With just three modes, the displacements are very well captured. There is no practical numerical difference between the 4 methods used to build the transformation matrix. If the basis of modes is not modified (i.e., the last mode is not replaced with the quantity $\bar{x}^{\text{pert}} - \bar{x}^{\alpha=0}$), then the convergence is very slow (results are omitted for brevity). This is not surprising, because a set of cantilevered modes cannot capture a rigid-body pitch motion well. If the basis is modified with just 5 modes, then the convergence is excellent (Fig. 8).

F. Test Model 1: Nonlinear Transient Analysis (Pure Structural Case)

The case presented here covers structural nonlinearity and concentrated applied loads applied at once and kept constant in time. The loads are applied at the tip of the wing. The correlation with Nastran is excellent (see Fig. 9). The time integration is carried out by using Newmark's method [58].

G. Test Model 1: Nonlinear Transient Analysis with Aerodynamic Effects Included

In Fig. 10, the results of simulations with three different values of $N_{\text{time step}}$ are presented. It is clear that with $N_{\text{time step}} > 8$, convergence

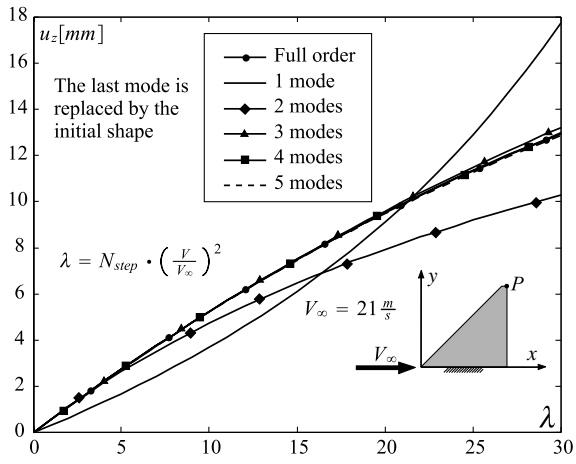

Fig. 8 Effect of the number of modes on the delta-wing full-order structure and reduced aerodynamic model; method 1 is used.

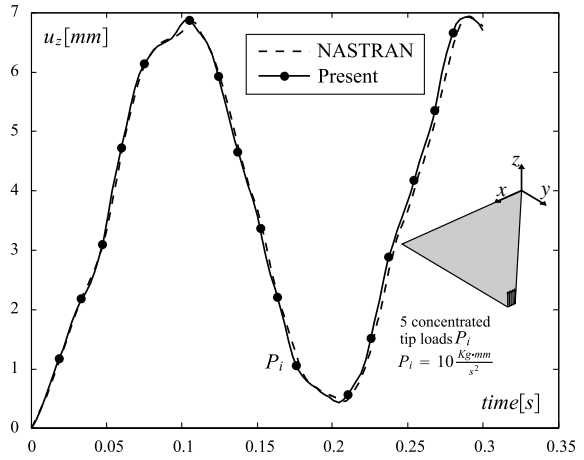

Fig. 9 Comparison with Nastran for out-of-plane tip displacement u_z (nonlinear transient analysis).

is reached and the aerodynamic forces are well-calculated. Note that the transformation matrix used to calculate the full-order aerodynamic matrices is calculated using method 1: the mass matrix is modified and the LSM is performed on the u_z displacement. In the steady case, we have demonstrated that there is not much difference between the 4 methods (see Table 2). For the cantilevered-wing cases presented here, it is crucial to replace the last modal shape of the modes used in the aerodynamic approximation by using the perturbed shape (in this case, the shape corresponding to a rigid pitching rotation of $\alpha = 1$ deg). It also should be noted that the flight speed is for the case of $\zeta_i = 0.01$ and $V_\infty = 21$ m/s. This speed is smaller than the linear flutter speed corresponding to the same damping ratio. Therefore, it is not surprising that the oscillations in Fig. 10 are damped.

The speed considered is applied all at once as a step input. The reference damping matrix is obtained by assigning viscous damping ratios to 20 natural modes (with no modified mass matrix). Using the LSM, a transformation is then carried out between these modes and 50 modes for which the generalized aerodynamic matrices are built. We will demonstrate later that for this case, only 5–10 modes are sufficient to well approximate the aerodynamics. The 50 modes used are built by using a modified mass matrix (method 1). The last modal shape is replaced with the quantity $\bar{x}^{\text{pert}} - \bar{x}^{\alpha=0}$, as for the steady case. The same 50 shapes are also used to build the transformation matrix from reduced modal order to full order. Method 1 is used and the LSM is performed on the component u_z. The damping matrix will subsequently be expanded to full order using the same transformation matrix used to expand the aerodynamic generalized

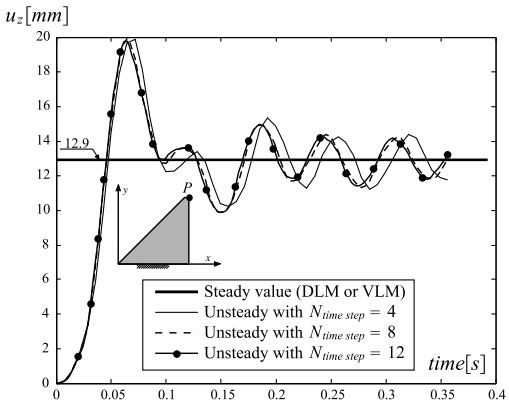

Fig. 10 Effect of the parameter $N_{\text{time step}}$ on the delta-wing transient response ($V_\infty = 21$ m/s). Aerodynamic generalized matrices are approximated using 50 modes and 6 lag terms. Method 1 is used and the last mode adopted for the aerodynamics is replaced with the shape corresponding to $\alpha = 1$ deg. The reference damping matrix is defined using 20 modes; $\zeta_i = 0.01$.

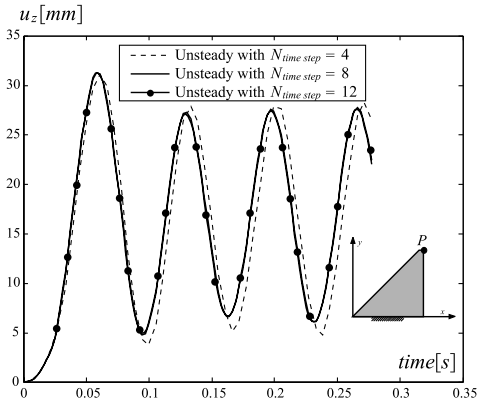

Fig. 11 Effect of the parameter $N_{\text{time step}}$ on the delta-wing postflutter response ($V_\infty = 27$ m/s). Aerodynamic generalized matrices are approximated using 50 modes and 6 lag terms. The reference damping matrix is defined using 20 modes; $\zeta_i = 0.05$.

matrices. In the formulation here, the transformation matrix and the generalized matrices are calculated using the same modes, which can be modified according to the 4 methods explained in the steady case.

A postflutter case is analyzed in Fig. 11. The transformation matrices and other parameters are the same as those used in the

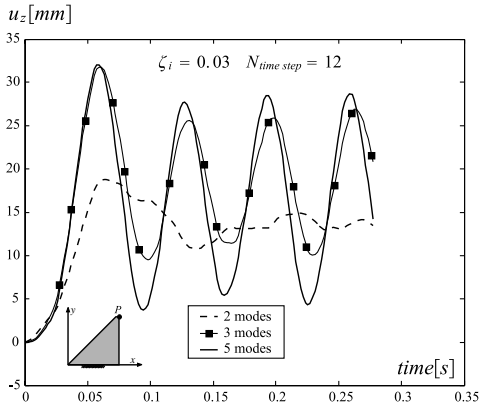

Fig. 12 Delta-wing postflutter LCO (tip displacement) ($V_\infty = 27$ m/s). Comparison of the results for aerodynamics approximated using 2, 3, and 5 modes and 6 lag terms. The reference damping matrix is defined using 2, 3, and 5 modes. Method 1 is used and the last mode adopted for the aerodynamics is replaced with the shape corresponding to $\alpha = 1$ deg; $\zeta_i = 0.03$.

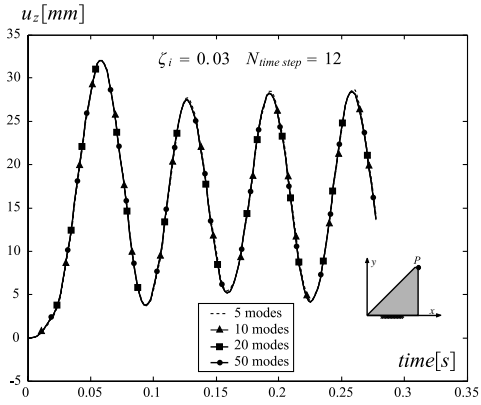

Fig. 13 Delta-wing postflutter LCO (tip displacement) ($V_\infty = 27$ m/s). Comparison of the results for aerodynamics approximated using 5, 10, 20, and 50 modes and 6 lag terms. The reference damping matrix is defined using 5, 10, 20, and 20 modes. Method 1 is used and the last mode adopted for the aerodynamics is replaced with the shape corresponding to $\alpha = 1$ deg.

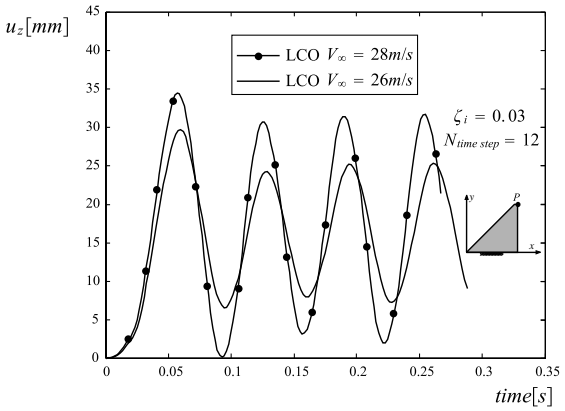

Fig. 14 Delta-wing postflutter LCO (tip displacement) ($V_\infty = 28$ and 26 m/s). Aerodynamic generalized matrices are approximated using 20 modes and 6 lag terms. The reference damping matrix is defined using 20 modes. Method 1 is used and the last mode adopted for the aerodynamics is replaced with the shape corresponding to $\alpha = 1$ deg.

derivation of Fig. 10. Again, it is demonstrated that $N_{\text{time step}} = 8$ or higher is sufficient to integrate the unsteady aerodynamic forces accurately. The wing responds in a limit cycle oscillation. The calculated LCO frequency (14.92 Hz) is in excellent agreement with Fig. 11 of [24]. The experimental value [24] of the LCO frequency is about 14.5 Hz. Because the damping coefficient has significant influence, and because it is not clear from [24] what damping coefficients were used, other tests to study the effect of changing the damping coefficient were needed. It was found that a value of $\zeta_i = 0.03$ led to good correlation with the experimental results.

The modal convergence of the approximation (tip displacement) is demonstrated in Figs. 12 and 13. With 5 modes, the convergence is practically achieved, as was demonstrated for the steady case (Fig. 8). It is important to consider other speeds and see the effect on the LCO amplitude and frequency. In Fig. 14, the LCO is plotted for the speeds $V_\infty = 28$ and 26 m/s. It is then necessary to verify if the nonlinear flutter speed and frequency are well correlated with the wind-tunnel results. For this flutter calculation, the modes used were not the same as those used to build the transformation matrix. In fact, in the generation of the transformation matrix, the modes are calculated using method 1 and the last shape is replaced by the quantity $\bar{\boldsymbol{x}}^{\text{pert}} - \bar{\boldsymbol{x}}^{\alpha=0}$. The modes used in the flutter analysis are just the natural modes obtained without modification of the mass matrix and without replacing the last modal shape. With the assumption of $\zeta_i = 0.03$, the linear flutter speed is $V_F^{\text{linear}} = 23.70$ m/s and the corresponding flutter frequency is $f_F^{\text{linear}} = 14.01$ Hz.

We now introduce the concept of consistent flutter speed and clarify what this terminology means. The linear flutter speed V_F^{linear} is calculated considering a basis of shapes (the modes in this paper). The modes are calculated by using the linear stiffness matrix of the

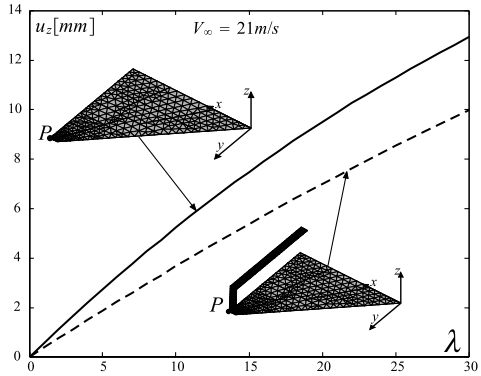

Fig. 15 Joined-wing and delta-wing with tip displacement [$P \equiv (a, 15/16a, 0)$ and $\alpha = 1$ deg] and full-order analysis for both structure and aerodynamics.

unloaded structure at the reference configuration with no angle of attack.

The consistent flutter speed $V_F^{\text{consistent}}$ is *not* the linear flutter speed. It is calculated as follows: a flow speed V'_∞, which is a candidate flutter speed, is assumed. Then the full-order static aeroelastic analysis, as earlier introduced, is performed. A deformed configuration will be the one corresponding to the nonlinear static equilibrium at the assumed flow speed V'_∞. At this point, the tangent matrix relative to this configuration is calculated and used to find the tangent modes. These tangent modes are now the shapes used for a *linear* flutter analysis, done as for the linear case. The used shapes in this case are relative to the deformed configuration. The flutter speed calculated with this method is called V'_F, which is generally smaller than V'_∞ if this speed was assumed to be sufficiently small. At this point, the procedure is repeated [64] by increasing the flutter-speed candidate.

Let V''_∞ be the new flutter-speed candidate. The new linearized flutter speed is found, determined using the modes of the static-equilibrium configuration at V''_∞. If this flutter speed V''_F is not equal to the flutter-speed candidate V''_∞, we repeat the procedure by increasing the candidate flutter speed. If, instead, $V''_F = V''_\infty$, then the consistent flutter speed is found: $V_F^{\text{consistent}} = V''_F = V''_\infty$. Therefore, the consistent flutter speed we use is defined as the speed at which the linearized structure about a steady equilibrium point loses stability at that point. That is, linearized generalized mass and stiffness matrices and mode shapes about this speed lead to the same speed as the linear flutter speed predicted by linear flutter analysis.

In the results presented here, with $\zeta_i = 0.03$ and 20 modes used for both the damping (the damping matrix is updated at the equilibrium configuration by calculating the tangent modes and using LSM) and aerodynamic generalized matrices, we have $V_F^{\text{consistent}} = 24.5$ m/s and $f_F^{\text{consistent}} = 14.5$ Hz, which are exactly coincident with the experimental data in [24].

It can be concluded that the viscous damping $\zeta_i = 0.03$ gives the best overall correlation with experimental results from the literature (flutter speed and frequency and LCO amplitude and frequency).

H. Delta Wing and the Corresponding Joined Wing: Full-Order Static and Linear Flutter Analyses

The effect on the static deflection of a tip point for the same speed V_∞ is shown in Fig. 15. The joined wing is stiffer than the corresponding separate delta wing. The linear flutter speed of this particular joined-wing configuration is considerably higher than that of the separate delta wing. In comparison with the delta wing (with flutter speed of 21.77 m/s and frequency of 15.21 Hz), the joined delta wing has a flutter speed of 32.98 m/s and a frequency of 13.52 Hz. It is assumed that $\zeta_i = 0.0$. These results are in excellent correlation with MD Nastran results. The convergence study of the linear flutter speed and frequency is reported in Table 3.

I. Test Model 2 Linear and Nonlinear Divergence Speeds

Linear divergence speed can be calculated by considering the unstable pole with zero reduced frequency in the *p-k* method (MD Nastran). It can also be calculated by solving an eigenvalue problem [65]. The *p-k* method (MD Nastran, 30 modes) gives $V_D = 78.38$ m/s, and the solution of an eigenvalue problem (MD Nastran) gives $V_D = 78.41$ m/s. Thus, no significant difference of the two methods is found.

Table 3 Joined-wing linear flutter speed and frequency convergence study with MD Nastran (in all cases, $\zeta_i = 0$)

Number of modes	Flutter speed, m/s	Flutter frequency, Hz
5	33.36	13.17
10	33.11	13.25
15	33.07	13.22
20	33.25	13.47
30	33.01	13.52
50	33.02	13.52

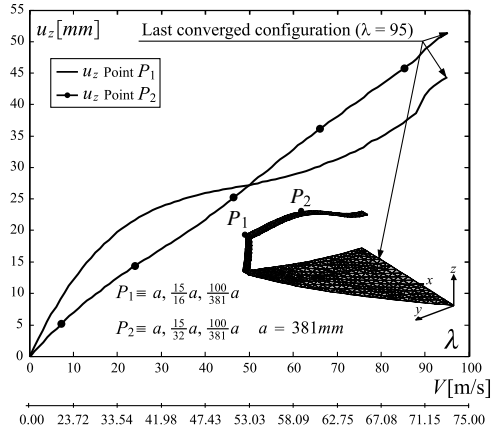

Fig. 16 Joined-wing nonlinear divergence speed calculation with full-order analysis for both structure and aerodynamics.

The divergence speed V_D can be properly calculated using a static nonlinear analysis as follows: the speed V_∞ and the number of load steps N_{step} are arbitrarily chosen. V_∞ should be higher than the predicted possible divergence speed: $V_\infty > V_D$; if it is not, no divergence speed will be found and so the speed has to be increased accordingly.

Once the parameters V_∞ and N_{step} are set, the Newton–Raphson procedure is applied as described in Sec. VIII. The divergence speed is the speed at which the aeroelastic tangent matrix [Eq. (68)] becomes *singular*. If λ_D is the load factor at which the aeroelastic tangent matrix $\boldsymbol{K}_{\text{tangent}}^{\text{step}\lambda\text{iter}n}$ becomes singular, the corresponding divergence speed can be estimated as follows:

$$\lambda_D \frac{\frac{1}{2}\rho_\infty V_\infty^2}{N_{\text{step}}} = \frac{1}{2}\rho_\infty V_D^2 \Rightarrow V_D = V_\infty \sqrt{\frac{\lambda_D}{N_{\text{step}}}} \tag{160}$$

The estimated divergence speed can be refined if the nonlinear analysis is performed with a new speed V_∞ close to the divergence speed estimated using Eq. (160).

In the present case, $V_\infty = 90$ m/s and $N_{\text{step}} = 100$. The singularity of the aeroelastic tangent matrix was found at $\lambda = \lambda_D = 68$. From Eq. (160), the first estimation of the divergence speed was then calculated and it was found to be $V_D = 74.22$ m/s. The calculation was then refined by setting $V_\infty = 75$ m/s and $N_{\text{step}} = 100$. For that case, $\lambda_D = 96$ was obtained. The

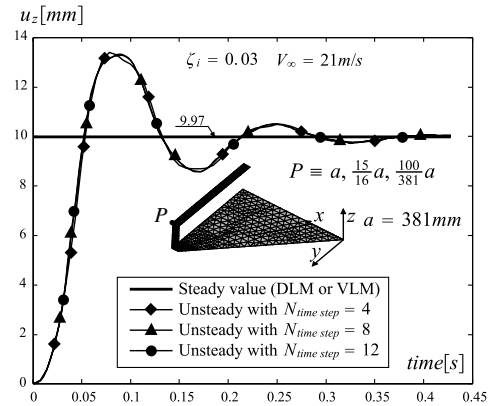

Fig. 17 Effect of the parameter $N_{\text{time step}}$ on the joined-wing transient response. Aerodynamic generalized matrices are approximated using 30 modes and 6 lag terms. The reference damping matrix is defined using 30 modes. Method 4 is used and the last mode adopted for the aerodynamics is replaced with the shape corresponding to $\alpha = 1$ deg. With this damping, the linear flutter speed is $V_F^{\text{linear}} = 33.68$ m/s and the linear flutter frequency is $f_F^{\text{linear}} = 13.06$ Hz. The linear flutter is calculated with the present capability using 20 modes.

corresponding refined estimation of the divergence speed was then $V_D = 73.48$ m/s [see Eq. (160)]. It can be concluded that this value is about 6% smaller than the linear divergence speed calculated using MD Nastran. Considering that the present calculation included the structural nonlinearity and so the actual stiffness, the nonlinear divergence speed is more likely to be the actual speed at which the static instability occurs. An experimental analysis should then be performed to validate the calculations. Also, more advanced techniques such as arc-length methods should be introduced to deal with limit points in a more efficient way.

The curve displacement vs load factor (and speed) is shown in Fig. 16 for two points on the rear wing.

J. Test Model 2 Nonlinear Transient Analysis of the Joined-Wing, Aerodynamic Effects Included

The time-domain simulation is performed for a speed smaller than the flutter and divergence speeds. In particular, $V_\infty = 21$ m/s is considered. As for the delta wing, the convergence is reached with $N_{\text{time step}} > 4$ and the aerodynamic forces are well calculated (see Fig. 17). Also, the convergence to the steady solution is clearly evident. After 0.5 s, the steady value is, in fact, reached. The basis $\mathbf{\Psi}$ is built by using natural modes and the LSM is performed on all the translational displacements u_x, u_y, and u_z (method 4). As for the case of the delta wing, the modal basis $\mathbf{\Psi}$ is modified by replacing the last mode with the initial shape.

XVI. Conclusions

A method for integrating generalized aerodynamic matrices is presented, obtained by standard linear unsteady aerodynamic codes for a modal base in the frequency domain, with full-order nonlinear structural finite element models. Consistency of formulation and results between the steady aeroelastic and unsteady aeroelastic cases is demonstrated. The idea is to use least-squares interpolation to create transformation matrices that allow (based on equivalent-work principles) expansion of modally reduced models to full-order finite element size. Full-order finite element analysis for general nonlinear structures capture their behavior well without the accuracy difficulties encountered by nonlinear structural modal approaches. The combination of full-order nonlinear finite element analysis with frequency-domain linear unsteady aerodynamics allows expansion into the nonlinear structural dynamics domain of methods that have been used successfully for years in the analysis, design, and clearance of practically all advanced aircraft flying today. Accuracy and consistency of the new formulation are demonstrated using a delta wing for which nonlinear numerical and experimental results are available.

The method presented here is general and capable of analyzing complex nonplanar structurally nonlinear configurations such as the joined-wing configurations.

References

[1] Boyd, W. N., "Effect of Chordwise Forces and Deformations and Deformations Due to Steady Lift on Wing Flutter," AIAA Paper 1979-794.

[2] Drela, M., "Method for Simultaneous Wing Aerodynamic and Structural Load Prediction," *Journal of Aircraft*, Vol. 27, No. 8, 1990, pp. 692–699. doi:10.2514/3.25342

[3] Drela, M., "Integrated Simulation Model for Preliminary Aerodynamic, Structural, and Control-Law Design of Aircraft," 40th AIAA/ASME/ASCE/AHS/ASC Structures, Structural Dynamics, and Materials Conference, St. Louis, MO, AIAA Paper 1999-1394, Apr. 1999.

[4] Livne, E., and Weisshaar, T. A., "Aeroelasticity of Nonconventional Airplane Configurations-Past and Future," *Journal of Aircraft*, Vol. 40, No. 6, 2003, pp. 1047–1065. doi:10.2514/2.7217

[5] Patil, M. J., Hodges, D. H., and Cesnik, C. E. S., "Nonlinear Aeroelastic Analysis of Complete Aircraft in Subsonic Flow," *Journal of Aircraft*, Vol. 37, No. 5, 2000, pp. 753–760. doi:10.2514/2.2685

[6] Patil, M. J., Hodges, D. H., and Cesnik, C. E. S., "Nonlinear Aeroelasticity and Flight Dynamics of High-Altitude Long-Endurance Aircraft," *Journal of Aircraft*, Vol. 38, No. 1, 2001, pp. 88–94. doi:10.2514/2.2738

[7] Cesnik, C. E. S., and Su, W., "Nonlinear Aeroelastic Modeling and Analysis of Fully Flexible Aircraft," 46th AIAA/ASME/ASCE/AHS/ASC Structures, Structural Dynamics and Materials Conference, Austin, TX, AIAA Paper 2005-2169, Apr. 2005.

[8] Wang, Z., Chen, P. C., Liu, D. D., Mook, D. T., and Patil, M. J., "Time Domain Nonlinear Aeroelastic Analysis for HALE Wings," AIAA Paper 2006-1640.

[9] Snyder, R. D., Hur, J. Y., Strong, D. S., and Beran, P. S., "Aeroelastic Analysis of High-Altitude Long-Endurance Joined-Wing Aircraft," 46th AIAA/ASME/ASCE/AHS/ASC Structures, Structural Dynamics and Materials Conference, Austin, TX, AIAA Paper 2005-1948, Apr. 2005.

[10] Patil, M. J., and Hodges, D. H., "On the Importance of Aerodynamic and Structural Geometrical Nonlinearities in Aeroelastic Behavior of High-Aspect-Ratio Wings," 41th AIAA/ASME/ASCE/AHS/ASC Structures, Structural Dynamics and Materials Conference, Atlanta, AIAA Paper 2000-1448, Apr. 2000.

[11] Sulaeman, E., Kapania, R., and Haftka, R. T., "Effect of Compressive Force on Flutter Speed of a Strut-Braced Wing," 44th AIAA/ASME/ASCE/AHS/ASC Structures, Structural Dynamics, and Materials Conference, Norfolk, VA, AIAA Paper 2003-1943, Apr. 2003.

[12] Sulaeman, E., Kapania, R., and Haftka, R. T., "Parametric Studies of Flutter Speed in a Strut-Braced Wing," 43rd AIAA/ASME/ASCE/AHS/ASC Structures, Structural Dynamics, and Materials Conference, Denver, CO, AIAA Paper 2002-1487, Apr. 2002.

[13] Sulaeman, E., "Effect of Compressive Force on Aeroelastic Stability of a Strut-Braced Wing," Ph.D Dissertation, Virginia Polytechnic Inst. and State Univ., Blacksburg, VA, Nov. 2001.

[14] Livne, E., "Aeroelasticity of Joined-Wing Airplane Configurations—Past Work and Future Challenges: A Survey," 42nd AIAA/ASME/ASCE/AHS/ASC Structures, Structural Dynamics, and Materials Conference, AIAA Paper 2001-1370, Seattle, WA, Apr. 2001.

[15] Wolkovitch, J., "The Joined Wing Aircraft: An Overview," *Journal of Aircraft*, Vol. 23, No. 3, 1986, pp. 161–178.

[16] Rasmussen, C., Canfield, R., and Blair, M., "Joined-Wing Sensor-Craft Configuration Design," 45th AIAA/ASME/ASCE/AHS/ASC Structures, Structural Dynamics and Materials Conference, Palm Springs, CA, AIAA Paper 2004-1760, Apr. 2004.

[17] Schwartz, J., Canfield, R., and Blair, M., "Aero-Structural Coupling and Sensitivity of a Joined-Wing Sensor Craft," 44th AIAA/ASME/ASCE/AHS/ASC Structures, Structural Dynamics, and Materials Conference, Norfolk, VA, AIAA Paper 2003-1580, Apr. 2003.

[18] Patil, M. J., "Nonlinear Aeroelastic Analysis of Joined-Wing Aircraft," 44th AIAA/ASME/ASCE/AHS/ASC Structures, Structural Dynamics and Materials Conference, Norfolk, VA, AIAA Paper 2003-1487, Apr. 2003.

[19] Lee, D., and Chen, P. C., "Nonlinear Aeroelastic Studies on a Joined-Wing with Wing Buckling Effects," 45th AIAA/ASME/ASCE/AHS/ASC Structures, Structural Dynamics and Materials Conference, Palm Springs, CA, AIAA Paper 2004-1944, Apr. 19–22, 2004.

[20] Rasmussen, C., Canfield, R., and Blair, M., "Optimization Process for Configuration of Flexible Joined-Wing," 10th AIAA/ISSMO Multidisciplinary Analysis and Optimization Conference, Albany, NY, AIAA Paper 2004-4330, Aug. 2004.

[21] Tang, D., Henry, J. K., and Dowell, E. H., "Limit Cycle Oscillations of Delta Wing Models in Low Subsonic Flow," *AIAA Journal*, Vol. 37, No. 11, 1999, pp. 1355–1362. doi:10.2514/2.627

[22] Tang, D., Dowell, E. H., and Hall, K. C., "Limit Cycle Oscillations of a Cantilevered Wing in Low Subsonic Flow," *AIAA Journal*, Vol. 37, No. 3, 1999, pp. 364–371. doi:10.2514/2.717

[23] Attar, P. J., Dowell, E. H., and White, J. R., "Modeling the LCO of a Delta Wing Using a High Fidelity Structural Model," 45th AIAA/ASME/ASCE/AHS/ASC Structures, Structural Dynamics and Materials Conference, Palm Springs, CA, AIAA Paper 2004-1692, Apr. 2004.

[24] Attar, P. J., Dowell, E. H., and White, J. R., "Modeling Delta Wing Limit-Cycle Oscillations Using a High-Fidelity Structural Model," *Journal of Aircraft*, Vol. 42, No. 5, Sept.–Oct. 2005, pp. 1209–1217.

[25] Geuzaine, P., Brown, G., Harris, C., and Farhat, C., " Aeroelastic Dynamic Analysis of a Full F-16 Configuration for Various Flight Conditions," *AIAA Journal*, Vol. 41, No. 3, 2003, pp. 363–371. doi:10.2514/2.1975

[26] Maute, K., Nikbay, M., and Farhat, C., "Coupled Analytical Sensitivity Analysis and Optimization of Three-Dimensional Nonlinear

Aeroelastic Systems," *AIAA Journal*, Vol. 39, No. 11, 2001, pp. 2051–2061.
doi:10.2514/2.1227

[27] Tang, D., and Dowell, E. H., "Experimental and Theoretical Study on Aeroelastic Response of High-Aspect-Ratio Wings," *AIAA Journal*, Vol. 39, No. 8, Aug. 2001, pp. 1430–1441.

[28] Peters, A. A., and Johnson, M. J., "Finite-State Airloads for Deformable Airfoils on Fixed and Rotating Wings," *Aeroelasticity and Fluid Structure Interaction Problems*, Vol. 44, edited by P. P. Friedmann, and J. C. I Chang, American Society of Mechanical Engineers, New York, Nov. 1994.

[29] Rodden, W. P., Taylor, P. F., and McIntosh, S. C., Jr., "Further Refinement of the Subsonic Doublet-Lattice Method," *Journal of Aircraft*, Vol. 35, No. 5, Sept.–Oct. 1998.

[30] Giesing, J. P., Kalman, T. P., and Rodden, W. P., "Subsonic Unsteady Aerodynamics for General Configurations," U.S. Air Force Flight Dynamics Lab. Rept. AFFDL-TR-71-5, Pt. 1, Vol. 1, Wright–Patterson AFB, OH, 1971.

[31] Rodden, W. P., Giesing, J. P., and Kalman, T. P., "New Developments and Applications of the Subsonic Doublet Lattice Method for Nonplanar Configurations," *Symposium on Unsteady Aerodynamics for Aeroelastic Analyses of Interfering Surfaces*, CP-80-71, AGARD Paper 4, 1970.

[32] Albano, E., and Rodden, W. P., "A Doublet Lattice Method for Calculating Lift Distributions on Oscillating Surfaces in Subsonic Flows," *AIAA Journal*, Vol. 7, No. 2, 1969, pp. 279–285.

[33] Kalman, T. P., Rodden, W. P., and Giesing, J. P., "Application of the Doublet Lattice Method to Nonplanar Configurations in Subsonic Flow," *Journal of Aircraft*, Vol. 8, No. 6, 1971, pp. 406–413.

[34] Richard, M., and Harrison, B. A., "A Program to Compute Three-Dimensional Subsonic Unsteady Aerodynamic Characteristics Using Doublet Lattice Method, L216 (DUBFLX)," NASA Langley Research Center, CR NAS 1-13918, Hampton, VA, Oct. 1979.

[35] Miller, R. D., Kroll, R. I., and Clemmons, R. E., "Dynamic Loads Analysis System (DYLOFLEX) Summary," NASA Langley Research Center, CR NAS 1-13918, Hampton, VA, Sept. 1979.

[36] Blair, M., "A Compilation of the Mathematics Leading to the Doublet-Lattice Method," U.S. Air Force Materiel Command, Flight Dynamic Directorate, Wright Lab., WL-TR-95-3022, Wright–Patterson AFB, OH, Nov. 1994.

[37] Sulaeman, E., "Discrete Element Methods for Calculating Aerodynamic Loadings on Lifting Surfaces in Unsteady Subsonic Flows," M.S. Thesis, Univ. of Dayton, Dayton, OH, Aug. 1993.

[38] Arendsen, P., "The B2000 Doublet Lattice Processor: B2-DL," National Aerospace Lab., Rept. TP-2002, Amsterdam, Oct. 2002.

[39] Magnus, A. E., and Epton, M. A., "PAN AIR-A Computer Program for Predicting Subsonic or Supersonic Linear Potential Flows About Arbitrary Configurations Using a Higher Order Panel Method," Vol. 1, NASA CR-3251, 1980.

[40] Chen, P. C., and Liu, D. D., "Unsteady Supersonic Computations of Arbitrary Wing-Body Configurations Including External Stores," *Journal of Aircraft*, Vol. 27, No. 2, Feb. 1990, pp. 108–116.
doi:10.2514/3.45905

[41] Chen, P. C., Lee, H. W., and Liu, D. D., "Unsteady Subsonic Aerodynamics for Bodies and Wings with External Stores Including Wake Effect," *Journal of Aircraft*, Vol. 30, No. 5, Sept.–Oct. 1993, pp. 618–628.

[42] ZAERO, Software Package, Ver. 7.1, ZONA Technology, Inc., Scottsdale, AZ, 2004.

[43] Demasi, L., and Livne, E., "The Structural Order Reduction Challenge in the Case of Geometrically Nonlinear Joined-Wing Configurations," 48th AIAA/ASME/ASCE/AHS/ASC Structures, Structural Dynamics and Materials Conference, Honolulu, HI, AIAA Paper 2007-2052, Apr. 2007.

[44] Demasi, L., and Livne, E., "Aeroelasticity of Structurally Nonlinear Lifting Surfaces Using Linear Modally Reduced Aerodynamic Generalized Forces," 47th AIAA/ASME/ASCE/AHS/ASC Structures, Structural Dynamics and Materials Conference, Newport, RI, AIAA Paper 2006-1639, May 2006.

[45] Levy, R., and Gal, E., "Triangular Shell Element for Large Rotations Analysis," *AIAA Journal*, Vol. 41, No. 12, 2003, pp. 2505–2508.
doi:10.2514/2.6854

[46] Levy, R., and Spillers, W. R., *Analysis of Geometrically Nonlinear Structures*, 2nd ed., Kluwer Academic, Boston, 2003.

[47] Gal, E., and Levy, R., "The Geometric Stiffness of Triangular Composite-Materials Shell Elements," *Computers and Structures*, Vol. 83, Nos. 28-30, 2005, pp. 2318–2333.
doi:10.1016/j.compstruc.2005.03.032

[48] Vivian, H. T., and Andrews, L. V., "Unsteady Aerodynamics for Advanced Configurations. Part 1: Application of the Subsonic Kernel Function to Nonplanar Lifting Surfaces," U.S. Air Force, Wright Dynamics Lab., TDR-64-152, Wright–Patterson AFB, OH, May 1965.

[49] Landahl, M. T., "Kernel Function for Nonplanar Oscillating Surfaces in a Subsonic Flow," *AIAA Journal*, Vol. 5, No. 5, May 1967, pp. 1045–1046.
doi:10.2514/3.55319

[50] Carson Yates, E., "A Kernel Function Formulation for Nonplanar Lifting Surfaces Oscillating in Subsonic Flow," *AIAA Journal*, Vol. 4, No. 8, 1966, pp. 1486–1488.
doi:10.2514/3.3722

[51] Ueda, T., "Expansion Series of Integral Functions Occuring in Unsteady Aerodynamics," *Journal of Aircraft*, Vol. 19, No. 4, Apr. 1982, pp. 345–347.
doi:10.2514/3.44758

[52] Mangler, K. W.,"Improper Integrals in Theoretical Aerodynamics," Royal Aircraft Establishment, Rept. 2424, Farnborough, England, U.K., 1951.

[53] Monegato, G., "Numerical Evaluation of Hypersingular Integrals," *Journal of Computational and Applied Mathematics*, Vol. 50, Nos. 1–3, 1994, pp. 9–31.
doi:10.1016/0377-0427(94)90287-9

[54] Stark, V. J. E., "Application of the Polar Coordinate Method to Oscillating Wing Configurations," Swenska Aeroplan AB Paper TN 69, 1973.

[55] Lottati, I., and Nissim, E., "Three-Dimensional Oscillatory Piecewise Continuous-Kernel Function Method, Part 2: Geometrically Continuos Wings," *Journal of Aircraft*, Vol. 18, No. 5, 1981, pp. 352–355.
doi:10.2514/3.57500

[56] Hedman, S. G., "Vortex Lattice Method for Calculation of Quasi Steady State Loadings on Thin Wings in Subsonic Flow," Aeronautical Research Inst. of Sweden, Rept. 105, Bromma, Sweden, 1965, pp. 5–17.

[57] Katz, J., and Plotkin, A., *Low-Speed Aerodynamics*, McGraw–Hill, New York, 1991.

[58] Bathe, K.-J., *Finite Element Procedures*, Prentice–Hall, Englewood Cliffs, NJ, 1996.

[59] Harder, R. L., and Desmarais, R. N., "Interpolation Using Surface Splines," *Journal of Aircraft*, Vol. 9, No. 2, 1972, pp. 189–192.
doi:10.2514/3.44330

[60] Dunn, H. J., "An Analytical Technique for Approximating Unsteady Aerodynamics in the Time Domain," NASA TP 1738, 1980.

[61] Roger, K. L., "Airplane Math Modeling Methods for Active Control Design," AGARD Rept. 228, Neuilly sur-Seine, France, 1977.

[62] Brase, L. O., and Eversman, W., "Application of Transient Aerodynamics to the Structural Nonlinear Flutter Problem," *Journal of Aircraft*, Vol. 25, No. 11, 1988, pp. 1060–1068.
doi:10.2514/3.45703

[63] Kreyszig, E., *Advanced Engineering Mathematics*, Wiley, New York, 1999.

[64] Demasi, L., and Livne, E., "Exploratory Studies of Joined Wing Aeroelasticity," 46th AIAA/ASME/ASCE/AHS/ASC Structures, Structural Dynamics and Materials Conference, Austin, TX, AIAA Paper 2005-2172, Apr. 2005.

[65] MSC.Nastran, Software Package, Ver. 68, MacNeal-Schwendler Corp., Los Angeles, CA, 1994.

C. Cesnik
Associate Editor